


## Driven Disordered Systems Approach to Biological Evolution in Changing Environments

Suman G. Das,<sup>1</sup> Joachim Krug<sup>1</sup> and Muhittin Mungan<sup>1,2</sup><sup>1</sup>*Institute for Biological Physics, University of Cologne, Zùlpicher Straße 77, D-50937 Köln, Germany*<sup>2</sup>*Institut für Angewandte Mathematik, Universität Bonn, Endenicher Allee 60, D-53115 Bonn, Germany* (Received 5 January 2022; revised 30 June 2022; accepted 3 August 2022; published 20 September 2022)

Biological evolution of a population is governed by the fitness landscape, which is a map from genotype to fitness. However, a fitness landscape depends on the organism's environment, and evolution in changing environments is still poorly understood. We study a particular model of antibiotic resistance evolution in bacteria where the antibiotic concentration is an environmental parameter and the fitness landscapes incorporate trade-offs between adaptation to low and high antibiotic concentration. With evolutionary dynamics that follow fitness gradients, the evolution of the system under slowly changing antibiotic concentration resembles the athermal dynamics of disordered physical systems under external drives. Exploiting this resemblance, we show that our model can be described as a system with interacting hysteretic elements. As in the case of the driven disordered systems, adaptive evolution under antibiotic concentration cycling is found to exhibit hysteresis loops and memory formation. We derive a number of analytical results for quasistatic concentration changes. We also perform numerical simulations to study how these effects are modified under driving protocols in which the concentration is changed in discrete steps. Our approach provides a general framework for studying motifs of evolutionary dynamics in biological systems in a changing environment.

DOI: [10.1103/PhysRevX.12.031040](https://doi.org/10.1103/PhysRevX.12.031040)Subject Areas: Biological Physics  
Interdisciplinary Physics  
Statistical Physics

## I. INTRODUCTION

The concept of the fitness landscape of a biological species, introduced by Wright [1], is a useful tool for understanding evolutionary processes. According to this picture, evolving populations are driven uphill along fitness gradients by natural selection. Mathematically, a fitness landscape is a map which assigns fitness values to genetic sequences. In recent decades, it has become feasible to empirically determine fitness landscapes comprising several mutations, and a wealth of new work has illuminated various aspects of evolutionary dynamics on different classes of fitness landscapes [2–10]. At the same time, the availability of empirical data has renewed the interest in studying fitness landscapes theoretically [11–16].

A less well-studied topic in this field is evolution in *changing* environments. Fitness landscapes are a function of environment, and can change in systematic ways as environmental parameters change. Whereas the fitness landscape provides information about  $G \times G$  (gene-gene)

interactions, the introduction of the environmental parameter furnishes information about  $G \times G \times E$  (where  $E$  stands for environment) interactions, i.e., about how the environment modifies the gene-gene interactions [17–20]. A few studies on microbial growth have measured or interpolated fitness values as a function of environmental parameters [21–23], but systematic theoretical work in this field is still limited.

Understanding and predicting the effect of the environment on fitness landscapes has important practical applications. A pertinent example is the case of antibiotic resistance in bacteria, where it has been shown that the fitness landscape depends strongly on the antibiotic concentration [21,22]. Uncontrolled variation in antibiotic concentration, both in clinical settings and elsewhere [24,25], is a cause for the rise in antibiotic resistance, which is a major clinical challenge today. Figure 1 shows an empirical example of the kind of processes we are interested in. The fitness values of the genotypes (i.e., genetic sequences) in the figure were measured in Ref. [21], and based on them one can predict transitions between genotypes under concentration increase (black and gray arrows) or decrease (red and orange arrows). Note that this small system already exhibits some interesting properties, such as a hysteresis loop under antibiotic concentration cycling and transient genotypes that are not part of the loop.

---

*Published by the American Physical Society under the terms of the Creative Commons Attribution 4.0 International license. Further distribution of this work must maintain attribution to the author(s) and the published article's title, journal citation, and DOI.*

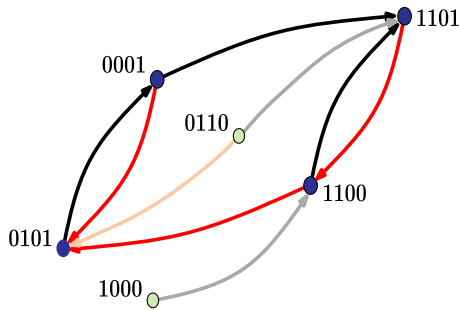


FIG. 1. State transition graph of antibiotic resistance evolution. The nodes depict genotypes composed of four mutations in the antibiotic resistance enzyme TEM-50  $\beta$ -lactamase. Genotypes are represented as binary strings where a 1 denotes the presence and 0 the absence of a specific mutation. The growth rates of bacteria expressing these mutant enzymes were reported in Ref. [21] for the antibiotic piperacillin at three different concentrations (128, 256, and 512  $\mu\text{g}/\text{ml}$ ). Each node is a local fitness maximum at one of these concentrations. Black and gray arrows connect nodes that would be reached under adaptive evolution when the concentration is increased, and red and orange arrows represent the dynamics under concentration decrease. For example, 0001 is a local maximum at 256  $\mu\text{g}/\text{ml}$ , but when the concentration is switched to 512  $\mu\text{g}/\text{ml}$ , it is no longer a fitness maximum. Evolution through a greedy adaptive walk (where every step is maximally fitness increasing) leads to the new maximum 1101. The graph displays a hysteresis loop 0101  $\rightarrow$  0001  $\rightarrow$  1101  $\rightarrow$  1100  $\rightarrow$  0101. The green nodes are transient and cannot be reached under cyclic concentration changes. Gray and orange arrows mark transitions out of transient states.

Our focus is primarily on antibiotic resistance evolution, where the environmental dependence of the fitness landscape is governed by a trade-off between two phenotypes, bacterial growth rate and resistance [23]. While we will mostly use the language of antibiotic resistance evolution in the following, the theory developed is more generally applicable, as will become clear from the mathematical model. Our work uses tools from statistical physics, specifically the physics of disordered systems. Concepts and methods from statistical physics have been used in the theory of evolution for a long time [26,27]. Precise quantitative analogies with evolutionary phenomena have been found with equilibrium statistical physics [28], the theory of random walks [29], spin glasses [30–32], and many more. Most of these, however, focus on static fitness landscapes.

Here we investigate evolution on rugged landscapes, i.e., landscapes with a large number of local fitness maxima, that vary with changes in an external parameter. This setting is naturally reminiscent of the physics of driven disordered systems, particularly in the athermal quasistatic regime [33], where thermal activation processes are absent or negligible. The primary effect of the external forcing is then to alter the set of stable equilibria or their locations. As a result, under a time-varying external forcing such systems

remain in a given equilibrium until it becomes unstable, and a fast relaxation process leads to a new equilibrium. Despite the absence of thermal activation processes, the resulting dynamics can nevertheless be rather complex, exhibiting memory effects [34,35] as well as dynamic phase transitions, such as the jamming transition in granular materials [36], or the yielding transition in amorphous solids [37].

In particular, we find that evolutionary genotypic change has close parallels with systems such as cyclically sheared amorphous solids [38,39], where a changing environmental parameter is analogous to an external shear, and transitions to new genotypes are similar to localized plastic events inside the solid which can exhibit hysteresis. As was shown recently [35,40,41], the athermal quasistatic conditions permit a rigorous description of the dynamics of such systems in terms of a directed *state transition graph*. Since the transition graph represents the response of the system to any possible deformation protocol, it provides a bird’s-eye view of the possible dynamics [35,42,43].

The main goal of this paper is to show that the driven disordered systems approach leads to new insights into evolution in changing environments, such as the prevalence of hysteresis, precise rules for the substitution of mutations along fitness-increasing paths in the rare-mutation regime, and the encoding of the evolutionary past in the genome. We establish new quantitative results, such as the number of fitness maxima across the entire permissible range of environmental parameters, the mean number of mutations that fix after an instability occurs, and the extent of reversibility of the adaptive evolution. Finally, we extend our results by going beyond the quasistatic limit, considering the adaptive response to discrete jumps in concentration. We find that several of our results carry over to this more realistic setting, but there are interesting differences as well when large jumps in concentration are involved.

Our analysis is carried out on a model of antibiotic resistance evolution. This model is based on empirical observations on the generic properties of dose-response curves obtained in the literature on drug resistance and provides a principled way of describing the environment dependence of fitness landscapes. This introduces a new dimension into the traditional study of fitness landscapes, which has mostly been concerned with a fixed environment. Exploiting the analogy with disordered systems, we find that the transition graphs describing the evolution of antibiotic resistance have a structure that bears strong resemblance to the Preisach model [44] of hysteresis in magnets, but in a generalized setting where the elementary units of hysteresis interact with each other [43,45–48]. Lastly, we believe that the disordered systems viewpoint, in particular the state transition graph approach, is a useful addition to the mathematical repertoire of evolutionary theory.

The paper is structured as follows. In Sec. II, we introduce the mathematical model and the central concepts

essential to its analysis. Section III contains the results and is divided into seven subsections. Sections IIIA–IIIC develop the formalism of state transition graphs and construct the set of local fitness maxima. Here we also derive several general results related to hysteresis and memory formation under quasistatic environmental change using this formalism. Section IIID provides statistical results regarding the number of local fitness maxima across environments, while Sec. IIIE reports numerical results on phenotypic reversibility, with statistical averages performed over evolutionary trajectories with quasistatically changing concentration. Section IIIF goes beyond the quasistatic approximation by studying dynamics under discrete changes in concentration. Section IIIG focuses on reversibility at the genotypic level and compares and contrasts it with phenotypic reversibility. Section IV summarizes the main results and discusses future directions for research.

## II. MODEL

We define a genotype  $\sigma$  as a binary string of length  $L$ , i.e.,  $\sigma_i \in \{0, 1\}$ , where  $i = 1, 2, \dots, L$  denotes the sites where mutations can occur, and  $\sigma_i = 1$  indicates the presence of a mutation. An equivalent and useful way of thinking about  $\sigma$  is as a set of mutations drawn from a total of  $L$  possible mutations. The genotype without mutations, commonly referred to as the *wild type*, is then the empty set, whereas the *all-mutant* is the set with all the  $L$  mutations. We will use the notation  $\sigma$  both as a string and as a set, and clarifications on the notation will be provided wherever necessary.

Our focus is on the trade-off-induced landscapes (TIL) model introduced in Ref. [23], which is defined through three key properties that are motivated by empirical observations. (1) The fitness of each genotype  $\sigma$  is a function of an environmental parameter  $x \geq 0$ , the antibiotic drug concentration, and is described by a fitness curve of the form

$$f_\sigma = r_\sigma w(x/m_\sigma). \quad (1)$$

The fitness curve thus has the same shape for different genotypes except for a rescaling of the axes by the genotype-specific parameters  $r_\sigma$  and  $m_\sigma$ . This is a common observation for various bacterial strains and antibiotics [23,49,50]. We call  $r_\sigma$  the null-fitness and  $m_\sigma$  the resistance of a genotype  $\sigma$ , following terminology used for bacterial *dose-response curves* that represent the population growth rate as a function of drug concentration [23,49,51]. We choose units such that for the wild type  $\sigma = \mathbf{0}$ ,  $r_{\mathbf{0}} = 1$ , and  $m_{\mathbf{0}} = 1$ , so that  $f_{\mathbf{0}}(x) = w(x)$ . Further,  $w(x)$  is a monotonic decreasing function, reflecting the decreasing fitness of a bacterial cell with increasing drug concentration. For numerical purposes, we will choose the widely used Hill function form:  $w(x) = 1/(1 + x^n)$ , where  $n$  is called the Hill exponent. Empirically obtained dose-response curves

are frequently fitted through Hill functions [51], and the scaling property expressed in Eq. (1) shows up as a common value of  $n$  shared by various mutants of the same strain exposed to the same drug [49,50]. (2) Every mutation comes with two parameters,  $r_i$  and  $m_i$ , and for any genotype,  $r_\sigma = \exp[\sum_i \sigma_i \ln r_i]$  and  $m_\sigma = \exp[\sum_i \sigma_i \ln m_i]$ . Thus, the effects of individual mutations combine in a simple multiplicative manner. This is based on empirical observation that phenotypes of null-fitness and resistance in fact exhibit limited or no epistasis for several microbial species and drugs [23,52,53]. (3) The mutations exhibit trade-off between adaptation to low and high drug concentrations [25,52,54]; i.e.,  $r_i < 1$  and  $m_i > 1$ . This means that every mutation enhances the resistance, but this comes at the cost of reduced null-fitness. The fitness curves of a specific realization of the TIL model with  $L = 2$  mutations are shown in Fig. 2(a).

The problem of analyzing this model has two components. First, one needs to understand the topography of the fitness landscape, i.e., the set of local fitness maxima and the paths that lead to the maxima, for a fixed  $x$ . The second part involves questions about evolutionary dynamics between maxima under changing drug concentrations. The first part has been addressed in detail in Ref. [23], and we describe some of the salient features of landscape topography here. The landscape of the TIL model is highly rugged (except at very low and very high  $x$ ); i.e., the number of fitness maxima is asymptotically exponential in  $L$  [23]. To describe evolutionary dynamics at fixed  $x$ , it is useful to introduce the notion of a *fitness graph*. The nodes of the fitness graph are the genotypes, and edges connect *mutational neighbors*, i.e., genotypes that differ by a single mutation. The fitness graph is an acyclic oriented graph, where the edges point toward increasing fitness [16,55]. The fitness graph depends on  $x$ : a fitness maximum for a certain value of  $x$  may not be a fitness maximum for another [see Fig. 2(b) for an example]. Note that the fitness graphs change only when the fitness curves of two mutational neighbors intersect. Evolution is assumed to proceed through adaptive walks; i.e., the entire population moves along the edges of the fitness graph respecting their orientation [30,56–59] (see Appendix A for further details). While this is an idealization, adaptive walks have been found useful in the analysis of microbial evolution experiments [60–62].

Along the path taken by an adaptive walk, the fitness increases monotonically, and such paths are therefore (*evolutionarily*) *accessible* [2,11,63]. The adaptive walk terminates once a local fitness maximum is reached. In general, there are multiple accessible paths starting from a genotype. A *greedy adaptive walk* is an adaptive walk in which every step is maximally fitness increasing [56]. A more realistic dynamics is obtained by assuming that the probability of a transition  $\sigma \rightarrow \sigma'$  is proportional to  $1 - e^{-2s}$  when  $s > 0$  and 0 otherwise, where  $s \equiv f_{\sigma'}/f_\sigma - 1$  denotes



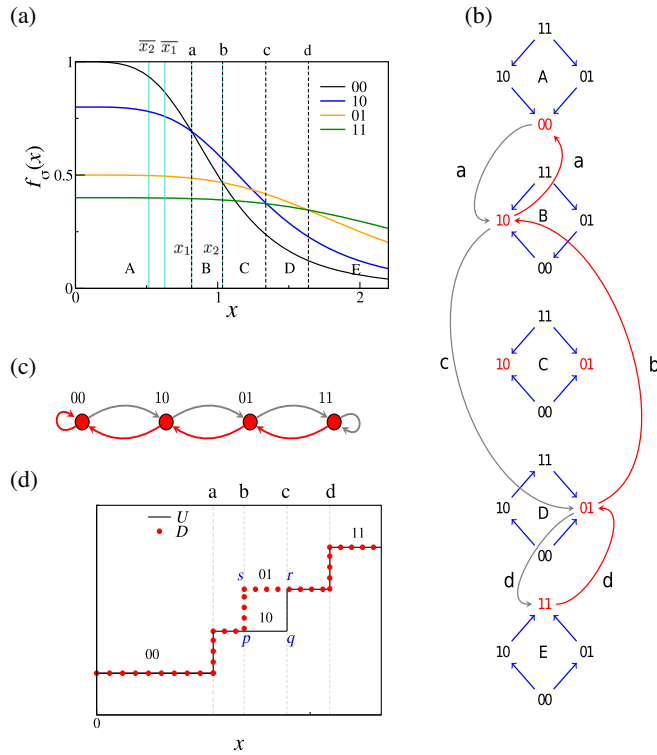


FIG. 2. Trade-off-induced fitness landscapes (TIL) model. (a) Fitness curves for four genotypes in a TIL model with two sites ( $L = 2$ ), with parameters  $r_1 = 0.8$ ,  $m_1 = 1.3$  and  $r_2 = 0.5$ ,  $m_2 = 2$ . The shape of the curve is the Hill function  $w(x) = 1/(1 + x^4)$  [49,51]. The figure is divided into five regions A–E, corresponding to different fitness graphs. A new fitness graph occurs when the fitness curves of two mutational neighbors intersect. The  $x$  values of the intersection points are marked by the letters a–d. The elements  $x_1, x_2, \bar{x}_1, \bar{x}_2$  of the ordering sequence (see main text) are indicated by solid vertical lines. (b) Fitness graphs in the regions A–E. Concentration  $x$  increases in the downward direction. In each fitness graph, the local fitness maxima (LFMs) are marked in red. Evolution in a fitness graph follows the oriented edges until a fitness maximum is reached. The curved gray arrows follow the evolution of the system under quasistatic increase of  $x$  starting from the stable state 00 at  $x = 0$  until the all-mutant 11 is reached; the curved red arrows continue the trajectory as the concentration is quasistatically decreased until 00 is reached again. (c) Transition graph for the two-site system is shown. This should be distinguished from the fitness graphs in (b). The nodes of the transition graph are the stable states which, in this simple case, comprise all genotypes. The gray arrows are the  $U$  transitions, i.e., the transitions under concentration increase, and the red arrows are the  $D$  transitions, i.e., transitions under concentration decrease. The transition graph can be read off from the sequence of fitness graphs in (b). (d) The transition between states is shown schematically. Each horizontal level is a genotype, and the vertical lines denote transitions. The black lines correspond to genotypes reached under  $U$  transitions (starting from 00 at  $x = 0$ ), while the line traced out by the red dots indicates the genotypes reached under  $D$  transitions (starting from 11 at large  $x$ ). The hysteresis loop  $pqrs$  is marked.

the selection coefficient [57,58]. We have used this version of the adaptive walk dynamics for all simulations, and the greedy walk has been used in the discussion of some topological properties of specific transition graphs.

We also make use of the notion of *mutationally directed* (or simply directed) paths, which are paths in the fitness graph along which the number of mutations relative to the wild type increases or decreases monotonically. The following interesting property about the TIL landscapes at fixed  $x$  was established in Ref. [23]. It is worth discussing, since we will use it to prove certain results in the following sections.

*Directed path accessibility.*—Given a fixed concentration  $x$ , every (mutationally) directed path ending at a local fitness maximum is accessible.

In other words, every local maximum  $\sigma$  is evolutionarily accessible from the subsets (supersets) of  $\sigma$  by a sequential gain (loss) of mutations; the mutations may be gained (or lost) in any order. This property has remarkable consequences. For example, the wild type is a subset of every genotype, and therefore can access every fitness maximum through all directed paths. Whenever the wild type is a fitness maximum, it must be the only fitness maximum in the landscape, since it can be accessed from all genotypes. The same two properties also hold for the all-mutant. With this background, we move on to the main focus of this article, which is evolutionary dynamics under slow changes in  $x$ . It is here that the relation with driven disordered systems, in particular the Preisach model, will become apparent.

### III. RESULTS

#### A. Stable states

We consider an evolutionary dynamic where the system is driven by changing the parameter  $x$ , and at each value of  $x$  we wait long enough so that the system reaches a local fitness maximum through an adaptive walk. An estimate of the necessary waiting time in terms of population-genetic parameters is provided in Appendix A. We call a genotype a *stable state* if it is a local fitness maximum (LFM) at some concentration  $x$ . As  $x$  changes, the fitness graph is altered by flipping the direction of one edge every time the fitness curves of two mutational neighbors intersect [see Figs. 2(a) and 2(b)]. A stable genotype  $\sigma$  ceases to be a LFM once its fitness curve intersects that of a mutational neighbor, and the system transitions to a new stable state by moving along the oriented edges of the new fitness graph.

Given a state  $\sigma$ , we define the two disjoint sets  $I^+[\sigma] = \{i: \sigma_i = 1\}$ ,  $I^-[\sigma] = \{j: \sigma_j = 0\}$ . For  $i \in I^+[\sigma]$ , we denote by  $\sigma^{-i}$  the configuration obtained from  $\sigma$  by setting  $\sigma_i = 0$ . Likewise, for  $j \in I^-[\sigma]$ , let  $\sigma^{+j}$  denote the configuration obtained from  $\sigma$  by setting  $\sigma_j = 1$ . Let  $x_i$  be the intersection point of the dose-response curves of the

wild type  $\sigma = \mathbf{0}$  and the genotype with a single mutation at site  $i$ , i.e.,  $\mathbf{0}^{+i}$ . Hence,  $x_i$  is the solution of the equation

$$w(x) = r_i w(x/m_i). \quad (2)$$

By a suitable choice of the function  $w(x)$  this solution can be guaranteed to be unique (see Ref. [23] and Appendix B). It then follows that for  $\sigma$  and  $i \in I^-[\sigma]$ , the fitness curves of  $\sigma$  and  $\sigma^{+i}$  intersect at  $m_\sigma x_i$ . Likewise, for  $j \in I^+[\sigma]$ , the fitness curves of  $\sigma$  and  $\sigma^{-j}$  intersect at  $m_\sigma \bar{x}_j$ , where we have defined  $\bar{x}_j = (x_j/m_j)$ . We now see that a necessary and sufficient condition for a genotype  $\sigma$  to be a stable state is that

$$\max_{j \in I^+[\sigma]} \bar{x}_j < \min_{i \in I^-[\sigma]} x_i. \quad (3)$$

If this holds, let the index  $\ell$  ( $u$ ) correspond to the site where the maximum (minimum) on the left-hand (right-hand) side of the inequality is attained. The stability range of  $\sigma$  is then  $(m_\sigma \bar{x}_\ell, m_\sigma x_u)$ . When starting from a genotype  $\sigma$  that is a LFM at  $x$ , the sites  $\ell$  and  $u$  are the first sites that undergo a mutation when decreasing, respectively increasing the concentration. We refer to sites  $\ell$  and  $u$  as the least-stable sites.

At this point, we introduce a fruitful analogy with the standard Preisach model, which is composed of a set of noninteracting two-level systems referred to as *hystérons* [44,64]. The mutation variable  $\sigma_i \in \{0, 1\}$  is analogous to the  $i$ th hysteron, and its states 0 and 1 correspond to the up and down states of the hysteron. The parameter  $x$  plays the role of an external magnetic field  $H$  that drives the system. In the Preisach model, each hysteron has an upper and lower threshold  $h_i^+$  and  $h_i^-$ , respectively. The  $i$ th hysteron remains in state 0 as long as  $H < h_i^+$ , and transits to 1 otherwise. Likewise, for  $H > h_i^-$  it remains in state 1, transitioning to 0 when this condition does not hold. Imposing for each hysteron that  $h_i^- < h_i^+$  implies that in the range  $(h_i^-, h_i^+)$  hysteron  $i$  can be in either of its two states. The particular state chosen is history dependent, giving thereby rise to hysteresis. Thus a necessary and sufficient condition for a hysteron configuration  $\sigma$  to be attainable at some magnetic field  $H$  is that

$$\max_{j \in I^+[\sigma]} h_j^- < \min_{i \in I^-[\sigma]} h_i^+, \quad (4)$$

which is identical to the TIL stability condition, Eq. (3). We thus define the *Preisach analog* of the TIL model as composed of  $L$  hystérons, where the upper and lower thresholds of the  $i$ th hysteron are  $h_i^+ = x_i$  and  $h_i^- = \bar{x}_i$ , respectively. Note that since  $m_i > 1$ , we have  $\bar{x}_i < x_i$ , so that the conditions Eqs. (3) and (4) are in fact equivalent, and we arrive at our first key result: The stable states of the TIL model and its Preisach analog are identical.

One immediate result following from the Preisach-TIL equivalence is the following proximity property of stable

states which holds for both models: if  $\sigma$  is a stable state, and  $\ell$  and  $u$  are its least-stable sites, then the genotypes  $\sigma^{+u}$  and  $\sigma^{-\ell}$  must be stable states as well. The proof follows by noting that if  $\sigma$  is stable and hence the inequality Eq. (3) holds, then by virtue of  $\bar{x}_i < x_i$ , this inequality must also hold for  $\sigma^{+u}$  and  $\sigma^{-\ell}$ . The proof of the proximity property is given in Appendix B.

For the Preisach model the proximity property implies the *no-avalanche condition* [64]: when  $H = h_u^+$ , we have a transition from  $\sigma$  to  $\sigma^{+u}$ , such that (i)  $\sigma^{+u}$  is a stable state by peak proximity, and moreover, (ii)  $\sigma^{+u}$  is a LFM at the field  $H = h_u^+$  that triggered the transition and hence no further state changes occur. An analogous result holds when  $H = h_\ell^-$ . However, while the proximity property (i) holds for the TIL model as well, the additional dependence on  $m_\sigma$  of the stability range  $(m_\sigma \bar{x}_\ell, m_\sigma x_u)$  of  $\sigma$  implies that (ii) will not hold in general. As we show next, this leads to significant differences in the dynamical properties of the two models. In particular, the TIL dynamics generically includes avalanches.

## B. Dynamics and the transition graph

In this section, we discuss dynamics under quasistatically changing  $x$ . While this assumption is not realistic in clinical applications, it is amenable to analytical treatment and provides a stepping stone toward more realistic protocols, which we consider in Sec. III F. Crucial aspects of the dynamics under quasistatically changing  $x$  can be described by transitions among stable states, such that the concentration is changed just enough so that the state ceases to be a LFM. We call such transitions under concentration increase a  $U$  transition, and that under concentration decrease a  $D$  transition. Then the dynamics can be described by a transition graph [see Fig. 2(c) for an example], where the nodes are the stable states, and each node has outgoing  $U$  and  $D$  edges corresponding to increasing and decreasing concentrations, respectively. This must be distinguished from a fitness graph, which is defined at a fixed concentration, and where the directed edges connecting mutational neighbors indicate the direction along which the fitness increases.

While the TIL model and its Preisach analog share the same set of stable states, the dynamical properties are, in general, different. To illustrate this, in Fig. 3 we show a particular realization of the TIL model with  $L = 5$  along with its Preisach analog. In the Preisach model, each transition comprises a single switching of the least-stable hysteron, which leads to a new stable state. In the TIL model, a change at a single site need not lead to a stable state. For example, the  $U$  transition  $15 \rightarrow 27$  in the TIL model in Fig. 3 involves changes at the third and fifth sites.

To understand why, first notice that under concentration changes in the  $U$  direction, the first change in a stable state  $\sigma$  [which must satisfy Eq. (3)] is a flip  $0 \rightarrow 1$  at the site  $u$  which has the smallest  $x_i$  among sites with  $\sigma_i = 0$ . This flip

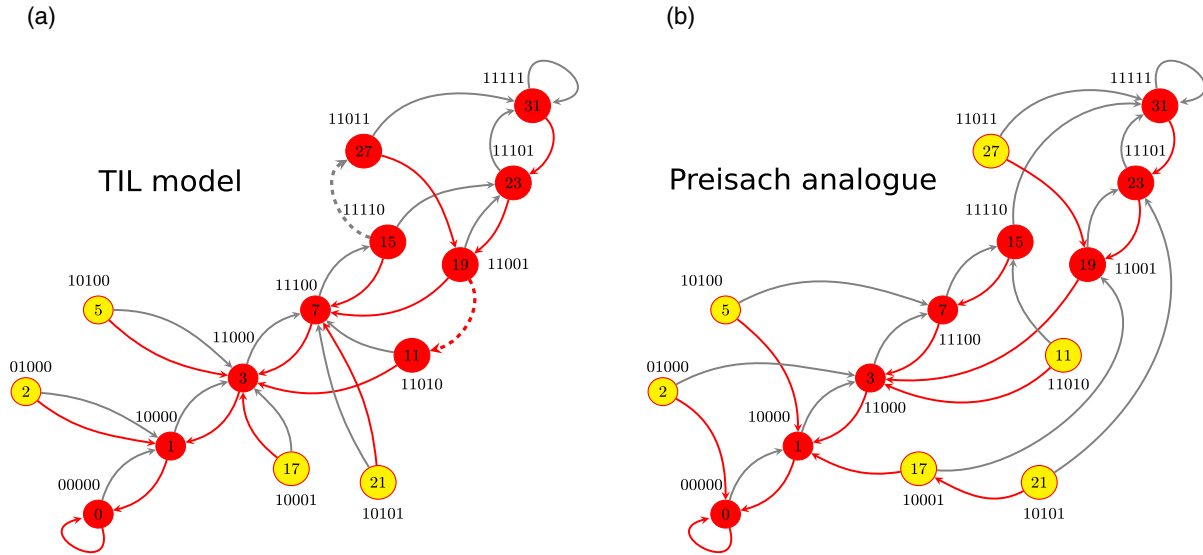


FIG. 3. Transition graph of a realization of the TIL model (a) and its Preisach analogue (b) with  $L = 5$  sites. The symbolic ordering sequence of this realization is given in Eq. (5). Each genotype is assigned an integer label, placed within the nodes, by interpreting the genotype string as a binary code where the leftmost digit is the least significant. The gray arrows are  $U$  transitions and red arrows are  $D$  transitions. The yellow nodes are the genotypes that cannot be reached starting from the wild type. When multiple outgoing arrows are present from a state, the solid ones correspond to greedy walks, whereas the dashed lines represent fitness-increasing walks but with one or more steps that are not maximally fitness increasing.

occurs at  $x = m_{\sigma}x_u$ . By the proximity property of the TIL model, the new state  $\sigma^{+u}$  is also stable, satisfying Eq. (3). However, in order for  $\sigma^{+u}$  to be a LFM at  $x = m_{\sigma}x_u$ , we must require that its lower stability threshold is less than or equal to  $x$ . This threshold is  $m_{\sigma^{+u}}\bar{x}_j = m_{\sigma}m_u\bar{x}_j$ , where  $j \in I^{+}[\sigma^{+u}]$  and  $\bar{x}_j > \bar{x}_k$  for all  $k \neq j$  with  $k \in I^{+}[\sigma^{+u}]$ . Therefore the new state is a fitness maximum if and only if  $m_u(\bar{x}_j/x_u) = (\bar{x}_j/\bar{x}_u) \leq 1$ , in which case the dynamics terminates at  $\sigma^{+u}$ . When the condition is violated, additional *secondary mutations* occur until a fitness maximum is reached. In the terminology of driven disordered systems, this corresponds to the occurrence of an avalanche. While many detailed properties of the secondary mutations depend on system parameters, certain features are general and in particular do not depend on the choice of  $w(x)$ . In the following we mention some of these.

In the Preisach model, exactly  $L$   $U$  transitions are required to get from the wild type to the all-mutant, and exactly  $L$   $D$  transitions to go from the all-mutant to the wild type, as is seen in Fig. 3. In the TIL model, due to the existence of secondary mutations, these numbers are generally different. The TIL model in Fig. 3 requires  $6U$  transitions to go from the wild type to the all-mutant, and  $6D$  transitions in the reverse direction, even though  $L = 5$ . One important consequence of the secondary mutations is that the number of mutations does not always increase monotonically under  $U$  or decrease monotonically under  $D$ . The first secondary mutation is always of a complementary kind to the initial mutation, where the changes  $0 \rightarrow 1$  and  $1 \rightarrow 0$  are defined to be of complementary kind to each

other (see Appendix B for a proof). Further mutations may also continue to be complementary to the initial mutation, leading to a (temporary) decrease in the number of mutations under  $U$  or an increase under  $D$ , as shown in a typical trajectory for  $L = 20$  mutations in Fig. 6(a). This seems counterintuitive, but arises from the state-dependent prefactor  $m_{\sigma}$  in the stability thresholds of stable states.

Moreover, when secondary mutations are present, the state  $\sigma'$  to which a transition occurs from a state  $\sigma$  need not be unique, due to the possible presence of multiple adaptive paths. In the TIL graph of Fig. 3, the state 15 can transition either to the state 27 or the state 23 under concentration increase. It can also be shown, using the property of direct path accessibility, that secondary mutations cannot cause a transition to a subset or superset of  $\sigma$  (see Appendix B); i.e., both the initial and the final state must contain at least one mutation not contained in the other. Another related consequence of the secondary mutations is that  $\sigma$  may transition to the same state  $\sigma'$  under  $U$  and  $D$  transitions. For example, the state 5 in the TIL graph in Fig. 3 transitions to the state 3 under both  $U$  and  $D$  transitions. This also appears counterintuitive from a biological standpoint, but it can occur when the stability range of  $\sigma$  is contained in that of  $\sigma'$ .

To understand the transition graph of the TIL model in a more systematic way, we adopt a strategy that has been fruitful for the Preisach model [64]. We construct a symbolic sequence  $p$  that specifies the total order among all the elements of  $\{x_i\}_1^L, \{\bar{x}_j\}_1^L$ . First, without loss of generality, we order our indices  $i$  such that  $x_1 < x_2 < \dots < x_L$ . Next, it is

useful to define the permutation  $\rho$  of  $(1, 2, \dots, L)$  that orders the  $\bar{x}_i$  among themselves from largest to smallest, so that  $\bar{x}_{\rho_1} > \bar{x}_{\rho_2} > \dots > \bar{x}_{\rho_L}$ . Since  $\bar{x}_i < x_i$  for each  $i$ , what remains is the specification of the ordering relation between  $\bar{x}_i$  and  $x_j$  for  $j \neq i$ . Given the sets  $\{x_i\}_1^L$ ,  $\{\bar{x}_j\}_1^L$  and the ordering prescribed by  $\rho$ , we can describe the total ordering in terms of a symbolic sequence  $p$  of elements  $\bar{i}$  and  $i$  by making the correspondence  $\bar{i} \leftrightarrow \bar{x}_i$  and  $i \leftrightarrow x_i$ , so that the sequence specifies the increasing order of  $x_i$  and  $\bar{x}_i$ . Since  $\bar{x}_i < x_i$  and the permutation  $\rho$  have to be respected, the sequence has to be such that the following hold: for each  $i$ ,  $\bar{i}$  is to the left of  $i$ ; the subsequence of sites without overbars is  $1, 2, \dots, L$ ; the subsequence of sites with overbars is  $\rho_L, \rho_{L-1}, \dots, \rho_1$ . As an example, consider the TIL model in Fig. 3, which has  $L = 5$ ,  $\rho = (43521)$  and the ordering

$$\bar{x}_1 < \bar{x}_2 < x_1 < \bar{x}_5 < \bar{x}_3 < x_2 < \bar{x}_4 < x_3 < x_4 < x_5.$$

The corresponding symbolic ordering sequence  $p$  is then

$$p = \bar{1} \ \bar{2} \ 1 \ \bar{5} \ \bar{3} \ 2 \ \bar{4} \ 3 \ 4 \ 5. \quad (5)$$

Because of the Preisach-TIL correspondence, whether a genotype or Preisach state is stable or not, and what the least-stable sites of a stable state are, can be read off from  $p$ , since the condition in Eq. (3) is easy to check by inspecting  $p$  (details are given in Appendix B). In the case of the Preisach model this implies that  $p$  completely determines the transition graph [64]. While this is not the case for the TIL model, the sequence  $p$  nevertheless contains considerable information about the TIL transition graph. In particular, this representation provides a precise condition for the existence of secondary mutations (see Appendix B): Secondary mutations are absent from all transitions in the TIL model if and only if the ordering sequence is of the form

$$p = \bar{1} \ 1 \ \bar{2} \ 2 \ \dots \ \bar{L} \ L. \quad (6)$$

In the absence of secondary mutations, the transition graph of the TIL model becomes identical to that of its Preisach analog. The transition graph in this case has a simple chain structure (see Fig. 4), and the number of stable states is  $L + 1$ , which is the lowest possible in a TIL (or Preisach) model. Note that despite identical transition graphs in this case, some dynamical differences are still present. Each Preisach element is hysteretic, and therefore forward and reverse transitions between two states do not occur at the same concentration; in the TIL model satisfying Eq. (6), however, they occur at the same concentration, namely the one at which the dose-response curves of the two genotypes intersect.

### C. Hysteresis, reversibility, and memory

The reversibility of evolution under a reversal of environmental conditions is an important question in evolutionary biology [65–67]. In the specific case of antibiotic resistance evolution, to what extent resistance is reversed in a drug-free environment is a question of considerable clinical importance [68–70]. One should note that different notions of reversion are used here. One common definition refers to a sudden (rather than slow) change in environment to a new state, followed by a switch back to the original state [68,71,72]. In the context of our model, we consider first reversion under quasistatic environmental changes, which would appear to be most conducive for approximately reversible behavior. The phenomenon of reversion is naturally linked to the notion of hysteresis under a slow and continuous change of an external field, and indeed the Preisach model was originally proposed as a simplified, tractable model of hysteresis in magnetic materials [44,64]. We then turn in Sec. III F to the possibility of reversion under jumplike concentration changes.

The TIL model also exhibits hysteresis and irreversibility. The highest degree of reversibility is exhibited by systems with chainlike transition graphs, such as in Fig. 2(c) or Fig. 4, where each transition  $\sigma \rightarrow \sigma'$  is accompanied by the transition  $\sigma' \rightarrow \sigma$  in the reverse direction, and there are no states with multiple outgoing edges in either direction. This means that under a reversal of the direction of concentration change, the same genotypes occur in reversed sequence. However, the transitions  $\sigma \rightarrow \sigma'$  and  $\sigma' \rightarrow \sigma$  need not occur at the same concentration. For example, in Fig. 2(d), the transition  $10 \rightarrow 01$  occurs at the point  $x = c$  during concentration increase, but  $01 \rightarrow 10$  occurs at  $x = b$  during concentration decrease. On the other hand, for systems of the type shown in Fig. 4, the forward and reverse transitions occur at the same concentration. However, such perfect reversibility is not typical of TIL models. The degree of reversibility depends on parameter choices. Figure 5 shows a realization of the TIL model with  $L = 5$  loci and a high degree of irreversibility, i.e., forward transitions with no corresponding reverse transitions, such as the  $D$  transition  $16 \rightarrow 1$  or the  $U$  transition  $15 \rightarrow 23$ .

Based on the observation of the systems described in Figs. 2 and 4, we need to distinguish between two kinds of hysteresis loops. We say that two states  $\sigma$  and  $\sigma'$  form a concentration loop if one can go from  $\sigma$  to  $\sigma'$  under quasistatic concentration increase and from  $\sigma'$  to  $\sigma$  under concentration decrease, and there is some range of  $x$  over

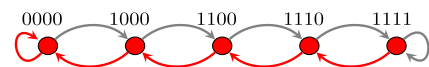


FIG. 4. TIL transition graph with  $L = 4$  and no secondary mutations. The ordering sequence is of the form given in Eq. (6). The transition graph is unique for this ordering sequence, and it is identical to the graph for the Preisach analog.



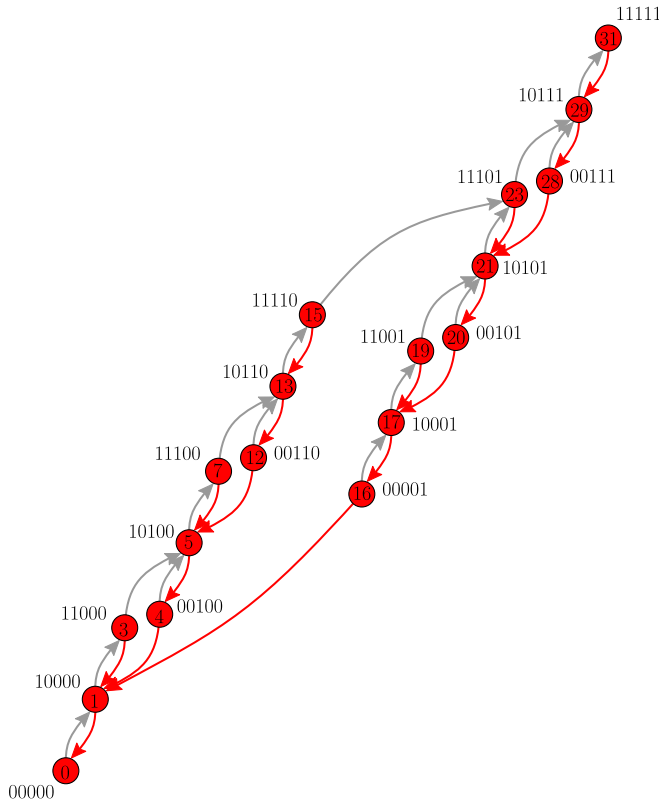


FIG. 5. TIL transition graph with  $L = 5$  and nested hysteresis loops. This graph was generated from a system with trade-off among all pairs of mutations, i.e., requiring that  $r_i < r_j \Leftrightarrow m_i > m_j$  for all  $i, j$ , and considering only transitions under greedy adaptive walks. The nesting of graph loops implies that genotypes can partially encode past changes of concentration. For example, starting from the wild type 0 at concentration  $x = 0$ , the genotype 19 can be realized only by increasing first the concentration enough in order to reach at least 23, followed by a decrease leading to at least 17 (but not further than 16) and a final increase of concentration.

which the forward and reverse trajectories do not share the same genotype. The system in Fig. 2 exhibits a concentration loop, as shown by the rectangle with corners marked by the points  $p, q, r$ , and  $s$  in Fig. 2(d). We say that  $\sigma$  and  $\sigma'$  form a graph loop ( $\sigma, \sigma'$ ) if one can go from  $\sigma$  to  $\sigma'$  under  $U$  transitions and from  $\sigma$  to  $\sigma'$  under  $D$  transitions, and if there is at least one genotype contained in either the forward or reversed sequence of states that is not contained in the other. A graph loop between two states implies a concentration loop, but a concentration loop does not imply a graph loop. For example, the case shown in Fig. 2 has a concentration loop, but does not have a graph loop, as can be seen in Fig. 2(c). An example of a graph loop in the TIL model in Fig. 3(a) is the one formed by the sequence of  $U$  transitions from 1 to 23 and the  $D$  transitions leading from 23 back to 1. A necessary condition for the existence of graph loops in the TIL model is the presence of secondary mutations; for otherwise, every transition must be among

mutational neighbors, and such that the upper stability threshold of one coincides with the lower stability threshold of the other, causing the transitions to be reversible.

Hysteresis is also linked to the notion of memory [34,35]. A genotype encountered along a trajectory not only contains information about the concentration, but also about the history of environmental change. At the simplest level, it may contain information about whether one is on the  $U$  or  $D$  boundary of a loop. For example, in the region between  $x = b$  and  $x = c$  in Fig. 2(d), the state 10 indicates that the concentration has been increasing, while 01 indicates that it was decreasing. But there is more information available than this, in general. The subloops seen in the TIL graphs in Figs. 3 and 5 contain (partial) information about extreme values of  $x$  reached in previous rounds of concentration cycling. For example, in the graph shown in Fig. 5, if the dynamics started with the wild type at  $x = 0$  and reached the genotype 19 at some point, one infers that the last transition happened by increasing the concentration to above the stability threshold of 17, but we also see from the transition graph that on some previous upward path the concentration must have exceeded the upper stability threshold of 15, followed by some sequence of transitions that brought it to the lower stability threshold of 16 for the first time since this happened.

In this context, it is important to mention the phenomenon of return-point memory (RPM) [40,73] possessed by certain systems. In our setting of adaptive evolution, RPM implies that genotypes at which the direction of the concentration change has been reversed can be returned to with a subsequent reversal and hence remembered. The RPM property is universally present in the Preisach model [34,40,64]. In the context of state transition graphs, one talks about the loop-RPM property, which ensures that the system cannot escape any loop between two states  $\sigma$  and  $\sigma'$  without passing through one of these states (see Refs. [40,64] for a detailed exposition). The RPM property implies the loop-RPM property, and is therefore possessed by the Preisach model and can be checked for the Preisach graph in Fig. 3.

Return-point memory is a mechanism by which a memory of local extremes of the driving parameter can be retained. For example, in the TIL model in Fig. 3(a) and under greedy dynamics, starting with the wild type at  $x = 0$ , and increasing the concentration until state 15 is reached, any decrease of concentration followed by a subsequent increase will eventually lead again to state 15. However, if the concentration continues to increase, so that state 23 is reached, then a concentration decrease to say 19 followed by an increase will not lead to 15 anymore. Thus the memory of 15 as the genotype at a local extreme event has been erased and replaced by 23. While we have found many realizations of the TIL model that possess the loop-RPM property under greedy transitions, such as the transition graphs shown in Figs. 3 and 5, it is not universally present.



Additionally, the existence of alternative fitness-increasing transitions, such as the ones shown in Fig. 3 by the dashed lines, can cause a loss of this kind of memory. To see this, consider the loop formed by the greedy  $U$  transitions leading from state 7 to 23 and the greedy  $D$  transitions going from 23 to state 7. On the downward trajectory from 23, it is possible to escape the loop without going first through 7 by making the transition  $19 \rightarrow 11$ .

#### D. Expected number of stable states

While many properties of the TIL model depend only on the ordering sequences  $\rho$  and  $p$ , for a more detailed study of the concentration-dependent evolutionary dynamics the fitness values of the model need to be explicitly assigned. In the standard Preisach model, one usually considers the thresholds to be independent random variables. Similarly for the TIL model, we assume that  $r_i$  and  $m_i$  follow a joint probability distribution with density  $P(r, m)$  and the ordered pairs  $(r_i, m_i)$  for  $i = 1, 2, \dots, L$  are independently and identically distributed. Their joint probability density is then given by  $Q(\{(r_i, m_i)\}) = \prod_{j=1}^L P(r_j, m_j)$ .

Since  $x_i$  and  $\bar{x}_i$  are functions of  $r_i$  and  $m_i$  only, the pairs  $(x_i, \bar{x}_i)$  for  $i = 1, 2, \dots, L$  are independently and identically distributed as well. Let the (marginal) cumulative distribution function of  $x_i$  be  $F_x(x_i)$  and that of  $\bar{x}_i$  be  $F_{\bar{x}}(\bar{x}_i)$ , and let  $P_{\bar{x}}(z) = F_{\bar{x}}'(z)$  denote the probability density function of  $\bar{x}_i$ . The probability that a genotype is a fitness maximum is the probability that Eq. (3) holds. The calculation of this probability is facilitated by the fact that  $I^+[\sigma]$  and  $I^-[\sigma]$  are disjoint sets. One can show that in the limit of large  $L$  the average number of stable states  $\langle N_{ss} \rangle$  is given by

$$\langle N_{ss} \rangle \simeq \sqrt{\frac{2\pi}{(L-1)|G''(z_0)|}} e^{G(z_0)(L-1)}, \quad (7)$$

where the average is taken with respect to  $Q(\{(r_i, m_i)\})$ ,  $G(z) = \ln[1 + F_{\bar{x}}(z) - F_x(z)]$ , and the global maximum of this function is at  $z_0$ . Thus the mean number of stable states is asymptotically exponential in  $L$ , showing the highly rugged nature of these landscapes [see Appendix C for the derivation of Eq. (7)].

#### E. Reversibility in the main hysteresis loop

An important dynamical question is understanding the evolutionary sequence of genotypes as the concentration is cycled between very low and very high values. We numerically generate trajectories starting from the wild type at  $x = 0$  and increasing  $x$  until the all-mutant is reached, and then decreasing  $x$  until the wild type is reached again. At each  $x$ , the system is evolved through the adaptive walk (based on selection coefficients, as discussed in Sec. II) until a LFM is reached. We call the trajectory composed of the sequences of LFMs the *main hysteresis loop*, and the

upward and downward parts of it the  $U$  and  $D$  boundary, respectively. The mean number of mutations in the genotype under quasistatic change in  $x$  on both the  $U$  and  $D$  boundaries is shown in Fig. 6(a), which clearly shows hysteresis. The inset shows a comparison with the Preisach model. Recall that in the TIL model the range of concentrations over which a genotype  $\sigma$  is a local maximum has an overall scale factor  $m_\sigma$ . Therefore, in order to facilitate comparison of the data for the TIL model and its Preisach analog, we have rescaled the concentration axis for the former by  $\langle m(x) \rangle$ , the average scale factor  $m_\sigma$  of the states  $\sigma$  that are stable at concentration  $x$ . From the inset of Fig. 6(a) we see that for the Preisach model the curve for the number of mutations on the  $U$  boundary lies below the corresponding curve for the  $D$  boundary. This effect can be understood qualitatively as follows. The intersection points along the  $U$  boundary are governed by the distribution of  $x_i$ , and those along the  $D$  boundary by the distribution of  $\bar{x}_i = x_i/m_i < x_i$ . As a result, the  $i$ th mutation is acquired at a larger  $x$  along the  $U$  boundary compared to where it is lost on the  $D$  boundary. More generally, for any randomly chosen pair of mutations  $i$  and  $j$ ,  $x_j$  tends to be higher than  $\bar{x}_i$  since all the  $m_i$ 's are larger than 1. The consequence is that the intersections along the  $U$  boundary tend to occur at larger values of  $x$  compared to the  $D$  boundary, making the curve for the number of mutations along the  $U$  boundary lower. Essentially the same effect is visible for the TIL model when the  $x$  values are rescaled by the value of  $\langle m(x) \rangle$  on the boundaries. When the rescaling is not done, the  $U$  boundary becomes higher, as seen in the main part of Fig. 6(a). The clue to understanding this comes from Fig. 6(b), which shows that the average resistance level  $\langle m(x) \rangle$  at given  $x$  is lower for the  $U$  boundary. Since the intersection points have the prefactor  $m_\sigma$  in the TIL model, this effect tends to make the intersection points along the  $U$  boundary occur at lower values of  $x$ . For our system, this effect is apparently strong enough to shift the curve of the number of mutations along the  $U$  boundary above that of the  $D$  boundary.

Generally, the changes of resistance level and mutation number have a complex mutual dependence, and these can vary between systems depending on the dose-response curve and the parameter distribution. However, certain asymptotic features that hold generically for stable states can be computed to leading order. For example, as shown in Appendix C, the mean number of mutations in a state that is stable at  $x$  scales asymptotically as  $\simeq (\ln x)/b$ , where the parameter  $b = \langle \ln m \rangle$ , and  $m$  is the resistance of an individual mutation. This is indicated by the brown dashed line in Fig. 6(a). At the same level of approximation, the mean level of resistance satisfies the relation  $\ln \langle m(x) \rangle \simeq \ln x$ , which is shown as a dashed brown line in Fig. 6(b). The inset of Fig. 6(b) displays the fitness as a function of  $x$ , which is seen to decline at a much lower rate than that of the wild type, as a consequence of the increasing level of resistance. Detailed derivations of these results are given in Appendix C.

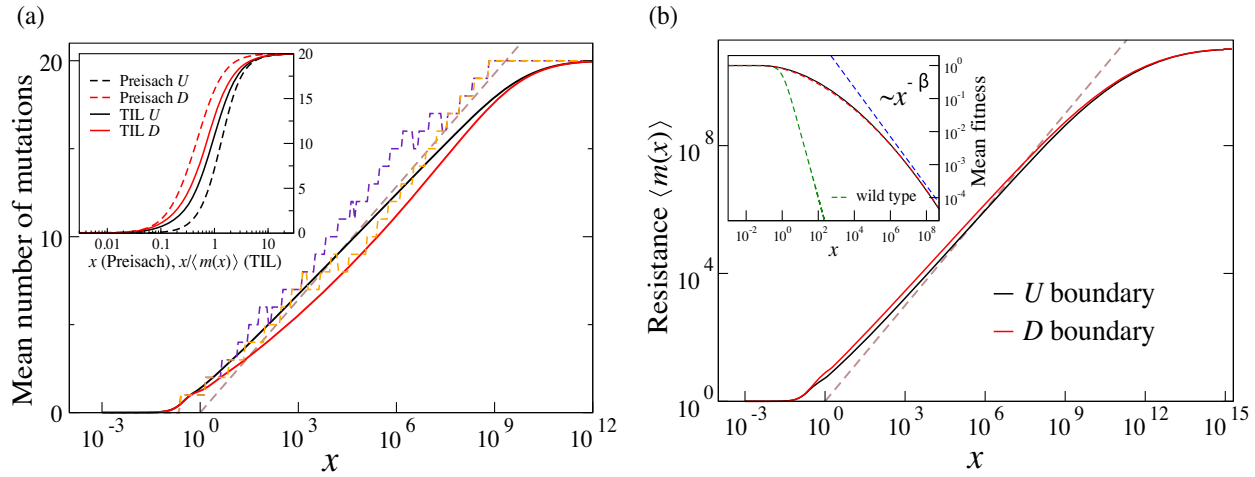


FIG. 6. Average properties of evolutionary trajectories along the main loop for  $L = 20$ . The dose-response curve is  $w(x) = 1/(1 + x^2)$ . The mutation parameters  $(r_i, m_i)$  are drawn randomly from a joint probability density described by Eqs. (C1) and (C2) in Appendix C. Adaptive walks (based on selection coefficients) were used for evolutionary dynamics. Greedy walks produce very similar results and are not shown. A total of  $10^4$  realizations were used to calculate averages. (a) Mean number of mutations in the genotypes along the  $U$  and  $D$  boundaries, which describe the behavior under increasing ( $U$ ) and decreasing ( $D$ ) concentrations. The dashed purple and orange lines show a typical sample trajectory. The dashed brown line is the curve  $(\ln x)/b$ , where  $b = \langle \ln m \rangle$ . The inset shows rescaled values of the mutation number in comparison to the Preisach analog (dashed lines). The rescaling is done by the mean resistance level  $\langle m(x) \rangle$ . (b) Mean resistance level  $\langle m(x) \rangle$  of the genotypes along the boundaries. The brown dashed curve is  $x$ . The inset shows the fitness of the genotypes along the boundaries. The dashed green line is the fitness of the wild type  $w(x)$ , and the dashed blue line is the power law  $x^{-\beta}$ , where  $\beta = -(a/b)$  and  $a = -\langle \ln r \rangle$ . Angular brackets denote averages over realizations.

**F. Beyond the quasistatic approximation**

For many applications, a more realistic driving protocol is one where  $x$  is changed discontinuously. Experiments on antibiotic resistance evolution often consider protocols where the concentration is changed stepwise by a constant factor [74,75]. To simulate this scenario, we numerically implemented a driving protocol where concentration is

sequentially increased in discrete steps from very low to very high values and then reversed. Both the increase and decrease occur by a factor of  $\langle m \rangle^\alpha$  in each step, and several values of  $\alpha$  were used. The limit  $\alpha \rightarrow 0$  corresponds to quasistatic driving. The results for the mean number of mutations along the  $U$  and  $D$  boundaries are plotted in Fig. 7(a). The hysteresis loops are thinner, implying a

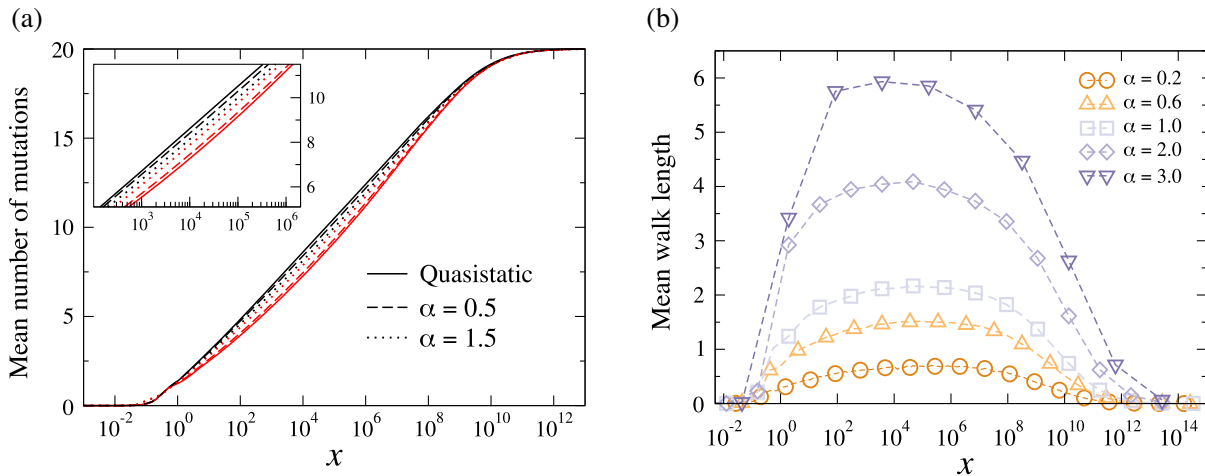


FIG. 7. Average properties of evolutionary trajectories along the main loop under finite driving rates  $\alpha$ . (a) Simulation results for the mean number of mutations along the main hysteresis loops have been plotted for different values of the jump sizes in concentration. The concentration has been changed in discrete steps by factor of  $\langle m \rangle^\alpha$ . The quasistatic case corresponds to the limit  $\alpha \rightarrow 0$ . The inset shows an enlarged version for clarity. (b) The length of adaptive walks has been plotted as a function of concentration for various values of  $\alpha$ . Adaptive walk lengths exceeding one step imply that secondary mutations have occurred.

higher phenotypic reversibility. When the concentration changes by a finite amount, the subsequent adaptive walk can move stochastically along multiple paths involving larger numbers of mutations [see Fig. 7(b)]. One therefore expects the system to reach a final distribution of phenotypes that depends less strongly on the starting point, consistent with higher reversibility on the phenotypic level (but not necessarily on the genotypic level, as we will see in the next section).

### G. Genotypic reversibility

Figure 8(a) shows simulation results with quasistatically changing  $x$  for the mean number of secondary mutations as a function of the number of background mutations (i.e., the number of mutations in the genotype from which the transition originates) along the main hysteresis loop. For large  $L$ , the number of secondary mutations depends weakly on the number of background mutations (unless the latter is close to 0 or  $L$ ). Moreover, as  $L$  increases linearly, the gaps between the curves decrease, indicating a possible asymptotic convergence toward a limiting shape (although this could not be verified conclusively). The number of secondary mutations is seen to be small, implying that adaptive walks at fixed  $x$  are short for quasistatic changes in  $x$ .

As was shown above, secondary mutations are also the source of genotypic irreversibility under quasistatic drive in the TIL model. We now describe a measure of genotypic irreversibility, adapted from a distance measure for evolutionary paths introduced in Ref. [76]. Let  $\sigma$  be the genotype at  $x$  on the  $U$  boundary of the main loop. Then  $d_U(x)$  is defined as the minimum of the Hamming distance between  $\sigma$  and the genotypes on the  $D$  boundary (for any concentration). The quantity  $d_D(x)$  can be defined in an analogous

way. The quantity  $\langle d_U(x) \rangle$  is plotted in Fig. 8(b). The distance measures vanish at very low and high concentrations, which is expected since the wild type and all-mutant are on both the  $U$  and  $D$  boundaries of the loop. The maximum value is reached close to the concentration at which the estimated mean number of mutations is  $L/2$ , as shown by the vertical dotted line. The level of reversibility is quite high for quasistatic driving, consistent with the low number of secondary mutations seen in Fig. 8(a). The quantity  $\langle d_D(x) \rangle$  shows very similar behavior (not shown).

We have also quantified the genotypic irreversibility for finite  $\alpha$  using the measure  $\langle d_U(x) \rangle$ , which is shown in Fig. 8(b). For large  $\alpha$ , the genotypic reversibility is lower, in contrast to the phenotypic reversibility in Fig. 7(a). The walk lengths increase with increasing  $\alpha$ , as shown in Fig. 7(b). The longer walks lead to higher genotypic divergence, even though the phenotypic properties of the LFMs that are accessed are very similar, as demonstrated in Fig. 7(a). Thus, even when there is substantial hysteresis at the genotypic level, one may still observe very similar levels of drug resistance evolving along the  $U$  and  $D$  boundaries. For small  $\alpha$ , we see from Fig. 8(b) that the maximum of  $\langle d_U \rangle$  is slightly lower than in the quasistatic limit. While the origin of this effect is not entirely clear, it is likely related to the fact that a small jump in concentration helps the system move beyond the quasistatic boundary and explore a slightly larger genotypic space. The trajectories would then be attracted preferentially toward a small number of nearby local maxima of high fitness, leading to these states evolving frequently along both the  $U$  and  $D$  boundaries. As  $\alpha$  increases, a larger number of maxima become accessible through the adaptive walk, leading to a larger dispersion and reduced recurrence of the final state.

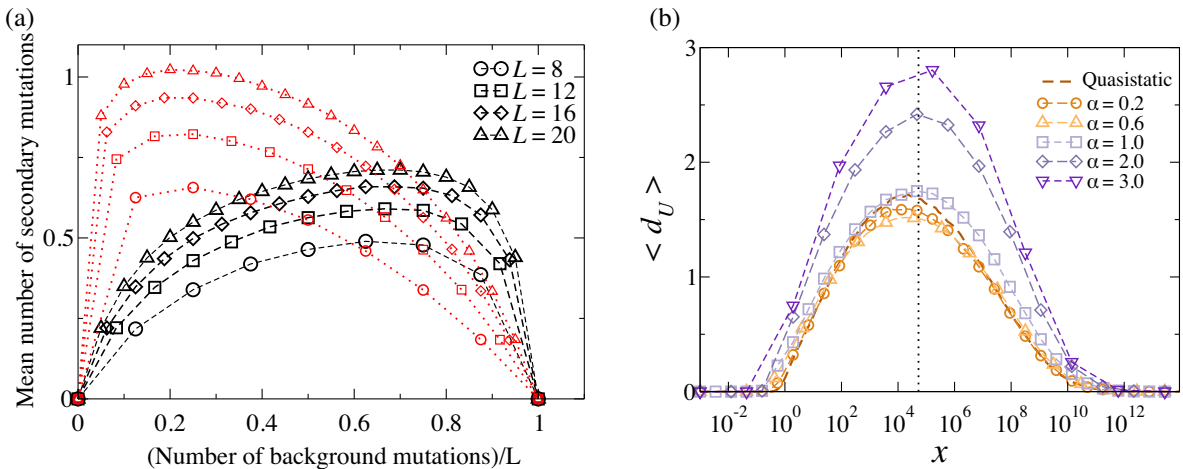


FIG. 8. Results on secondary mutations and genotypic reversibility. Simulations were conducted along the main hysteresis loop, and the mutation parameters were generated randomly as described in the main text and Appendix C. (a) The mean number of secondary mutations in an evolutionary transition under quasistatic driving as a function of the number of mutations in the originating background genotype. We used  $10^5$  realizations for averaging. Black symbols correspond to the  $U$  boundary and red to the  $D$  boundary. (b) Mean path irreversibility  $\langle d_U(x) \rangle$  is shown for various values of the driving rate  $\alpha$ . Averages were performed over  $10^4$  realizations. The dashed black line corresponds to the quasistatic limit  $\alpha \rightarrow 0$ .

#### IV. SUMMARY AND DISCUSSION

We have investigated a class of models of bacterial evolution under changing drug concentrations, and shown that their dynamics are closely related to those of driven disordered systems, exhibiting dynamical phenomena such as hysteresis and memory formation. As in the case of driven disordered systems, a state transition graph captures the dynamics of adaptive evolution in a changing environment. As a result, questions about evolution can be cast as questions about the graph topology. We have shown that in such models partial information about the changing environment is stored in evolving genotypes. Although our analysis has focused on the relatively simple TIL model, we should emphasize that the memory effects described here are generic features of disordered systems.

Specifically, we have found that the transitions between genotypes in a homogeneous population exhibit a number of generic properties which we have described in detail. In particular, adaptive walks are found to be short, i.e., they involve a small number of mutations, when a slow change in the drug concentration renders a LFM unstable. In this regime, the dynamics are not qualitatively altered by the precise nature of the adaptive walk. Moreover, the systems generically exhibit hysteresis loops, i.e., a lack of reversibility when the direction of concentration change is reversed. Conceptually, our work highlights the distinction between genotypic and phenotypic hysteresis. Genotypic reversibility is found to be low for concentration changes with large jumps. However, the degree of phenotypic reversibility is found to be rather high under driving protocols involving both small and large jumps in the environmental parameter. Thus, the phenotypes are similar along both the upward and downward boundaries of drug concentration cycling. We have obtained asymptotic scaling approximations to phenotypes such as the number of mutations and the fitness and resistance levels as a function of drug concentration. These are relatively robust to modifications in the driving protocol, making them easily accessible to empirical testing.

Under slow concentration changes, we find that the genotypic hysteresis loops in several instances of our model exhibit perfect or near-perfect return-point memory, i.e., the capability to return to a previously visited genotype at which the direction of concentration change was reversed. Although not universally present, existence of RPM is relevant to applications such as the emergence of antibiotic resistance, since it implies that drug concentration cycling can lead to reversal of resistance. The degree of reversibility, including the presence of RPM, is affected by the distribution of the effects of mutations on the null-fitness and resistance phenotypes. However, empirical knowledge regarding the distribution of these mutational effects is still limited. Moreover, our model assumes as an approximation that the mutations combine nonepistatically, which rules out phenomena such as the occurrence of compensatory

mutations that reduce the cost of resistance. Further work is needed to understand how various aspects of reversibility and memory are affected by these factors.

From a broader perspective, our work introduces a systematic approach to understanding how the information about a changing environment is encoded in the genotypes of a population. A possible direction for future research is the development of algorithms that infer features of the environmental history from the knowledge of evolved genomes using the state transition graph. Conversely, our approach can be used to design treatment protocols that are optimized to avoid or slow down the evolution of drug resistance by controlling the drug concentration or by cycling different antibiotics [77,78].

#### ACKNOWLEDGMENTS

We wish to thank two anonymous reviewers for their useful comments on an earlier version of the manuscript. S. G. D. and J. K. acknowledge support by the Deutsche Forschungsgemeinschaft (DFG, German Research Foundation) within SFB 1310 *Predictability in evolution*. M. M. was supported by the DFG under Projects No. 398962893, No. 211504053–SFB 1060, and under Germany’s Excellence Strategy–GZ 2047/1, Project No. 390685813.

#### APPENDIX A: ADAPTIVE WALKS AND CHANGING ENVIRONMENT

Adaptive walks describe the evolutionary dynamics in a limiting regime of strong selection and weak mutation [57,79]. Here *strong selection* implies that only beneficial mutations can fix, and *weak mutation* implies that no more than two genotypes are present in the population at any time. The timescale over which new beneficial mutations arise is  $t_{\text{mut}} = 1/(N\mu)$ , where  $N$  is the population size and  $\mu$  is the mutation rate per genome per generation. The timescale for fixation of a beneficial mutation is  $t_{\text{fix}} = s^{-1} \ln(N^2s)$  [80], where  $s > 0$  is the selection coefficient of the beneficial mutation. The weak mutation condition requires that  $t_{\text{fix}} \ll t_{\text{mut}}$ , which implies

$$N\mu \ln(N^2s) \ll 1. \quad (\text{A1})$$

In addition, we use the strong selection condition, where the fixation probability  $1 - e^{-2s}$  for beneficial mutations is derived from the well-known Kimura formula [81] in the limit

$$Ns \gg 1. \quad (\text{A2})$$

In our work, we have studied protocols in which we hold the concentration fixed for a waiting time  $t_{\text{wait}}$  until a LFM is reached. Since this involves several evolutionary steps, a necessary condition on the waiting time is  $t_{\text{wait}} \gg t_{\text{fix}}$ .



This condition is approximately satisfied in experimental evolution protocols where the drug concentration is increased by a constant factor whenever the bacterial cell density has recovered a predetermined level, signaling that a new fitness maximum has been reached; see Ref. [75] for a recent example. The adaptive walk approximation requires in addition the condition Eq. (A1), which was not the case in Ref. [75], but could be achieved by working at smaller population sizes.

## APPENDIX B: TIL-PREISACH EQUIVALENCE

We derive first some results for the TIL model which will be used in the following sections. These results are general in the sense that they do not depend on the shape of the dose-response function  $w(x)$  as long as it satisfies the following properties.

- (W1)  $w(x)$  is a continuous, strictly decreasing function for  $x \geq 0$ .
- (W2) For all pairs of permissible values  $(r, m)$  such that  $r < 1$  and  $m > 1$ , the curves  $w(x)$  and  $rw(x/m)$  intersect at precisely one point.

As noted in Ref. [23], these conditions are satisfied for a large class of dose-response functions considered in the literature, including the exponential and half-Gaussian functions. When considering statistical results, we will specialize to the  $n = 2$  Hill-type dose-response function  $w(x) = 1/(1 + x^2)$ . In this case, in order for (W2) to be satisfied, the permissible pairs  $(r, m)$  have to satisfy also  $m^2 r > 1$ .

As given in the main text, the stability condition of a state of the TIL model is

$$\max_{j \in I^+[\sigma]} \bar{x}_j < \min_{i \in I^-[\sigma]} x_i. \quad (\text{B1})$$

In the following, we shall assume that we are given a stable genotype  $\sigma$  such that

$$x^-[\sigma] = m_\sigma \bar{x}_\ell \quad \text{and} \quad x^+[\sigma] = m_\sigma x_u \quad (\text{B2})$$

hold with  $x^-[\sigma] < x^+[\sigma]$ , implying that the stability condition Eq. (B1) is satisfied, and the sites  $\ell$  and  $u$  are those at which the maximum (minimum) of the terms on the left- and right-hand side of the inequality are attained. We say that sites  $\ell$  and  $u$  are the least stable sites in the sense that the first mutation will occur there under concentration decreases or increases, respectively. The stability range of  $\sigma$  is then given as  $(x^-[\sigma], x^+[\sigma])$ .

By setting  $h_i^- = \bar{x}_i$  and  $h_i^+ = x_i$ , the condition (B1) becomes the stability condition for hysteron configuration  $\sigma$  of the Preisach model, as derived in the main text. The stability range  $(h^-[\sigma], h^+[\sigma])$  is then given by

$$h^-[\sigma] = \bar{x}_\ell \quad \text{and} \quad h^+[\sigma] = x_u, \quad (\text{B3})$$

which formally can be obtained from the stability range of its corresponding TIL state, Eq. (B2), by setting  $m_\sigma = 1$ . Thus while a TIL model and its Preisach analog have identical sets of stable states, the stability ranges of the two are different in general.

### 1. Proximity property of stable states

Given a stable TIL-Preisach state  $\sigma$ , we let again  $\ell$  and  $u$  denote its least-stable sites. The following result holds for the stability ranges  $h^\pm[\sigma]$  of the Preisach model:

$$h^-[\sigma] \leq h^-[\sigma^{+u}] < h^+[\sigma] < h^+[\sigma^{+u}], \quad (\text{B4})$$

$$h^-[\sigma^{-\ell}] < h^-[\sigma] < h^+[\sigma^{-\ell}] \leq h^+[\sigma]. \quad (\text{B5})$$

Note that these inequalities establish in particular that  $h^-[\sigma^{+u}] < h^+[\sigma^{+u}]$  and  $h^-[\sigma^{-\ell}] < h^+[\sigma^{-\ell}]$ , so that  $\sigma^{+u}$  and  $\sigma^{-\ell}$  are stable Preisach states as well. But by the TIL-Preisach equivalence they must be stable TIL states, too. This can also be seen by noting that the corresponding stability ranges are obtained from those of its Preisach analog by multiplication by  $m_{\sigma^{+u}}$  ( $m_{\sigma^{-\ell}}$ ). This is the proximity property of the stable states for the TIL model and its Preisach equivalent.

We only prove the inequalities in Eq. (B4); the proof of Eq. (B5) is similar. First, note that  $I^+[\sigma]$  is a proper subset of  $I^+[\sigma^{+u}]$ , and likewise  $I^-[\sigma^{+u}]$  is a proper subset of  $I^-[\sigma]$ . Since each of the two sets  $\{h_i^\pm\}_{i=1}^N$  is assumed to have distinct elements, it follows that

$$\min_{j \in I^-[\sigma^{+u}]} h_j^+ > \min_{j \in I^-[\sigma]} h_j^+. \quad (\text{B6})$$

Thus  $h^+[\sigma^{+u}] > h^+[\sigma]$  and the rightmost inequality of Eq. (B4) has been proven. Next, consider  $h^-[\sigma^{+u}]$  and particularly its least-stable element  $k$  under field decreases. Recall that we denoted the corresponding element for  $\sigma$  as  $\ell$ . Therefore, either (i)  $k = \ell$  or (ii)  $k = u$ . In the former case, it must have been that  $h_u^- < h_\ell^-$ , and therefore  $h^-[\sigma^{+u}] = h^-[\sigma] = h_\ell^-$ . In the latter case, the opposite must be true; i.e.,  $h_u^- > h_\ell^-$ , and therefore  $h^-[\sigma^{+u}] = h_u^- > h^-[\sigma]$ . Combining these two cases, it follows that  $h^-[\sigma^{+u}] \geq h^-[\sigma]$ , thereby establishing the leftmost inequality of Eq. (B4). However, since by definition  $h_u^- < h_u^+$ , in both cases it must be that  $h^-[\sigma^{+u}] < h^+[\sigma] = h_u^+$ , thereby establishing the middle inequality of Eq. (B4).

### 2. Construction of stable states from the symbolic order sequence $p$

Here we provide an explicit construction of the set of stable states of the TIL model (and its Preisach equivalent) from the symbolic order sequence  $p$ , which represents the ordering of the  $2L$  concentrations  $\bar{x}_i$  and  $x_j$ . Denoting the set of stable states associated with  $p$  as  $\mathcal{S}_p$ , this set can be

partitioned into the subset of states  $\mathcal{S}_{p,u}$  whose least-stable site under concentration increases is  $u$ , with  $u = 1, 2, \dots, L$  (this subdivision leaves out the all-mutant  $\sigma = \mathbf{1}$ , which is always stable, and we assign it to the singleton set  $\mathcal{S}_{p,L+1}$ ).

To illustrate the construction of  $\mathcal{S}_{p,u}$ , consider the order sequence (5) of the example given in the main text:

$$\begin{aligned} \bar{x}_1 < \bar{x}_2 < x_1 < \bar{x}_5 < \bar{x}_3 < x_2 < \bar{x}_4 < x_3 < x_4 < x_5, \\ \Leftrightarrow \\ p = \bar{1} \ \bar{2} \ 1 \ \bar{5} \ \bar{3} \ 2 \ \bar{4} \ 3 \ 4 \ 5. \end{aligned} \quad (\text{B7})$$

Let us construct  $\mathcal{S}_{p,2}$ , the set of stable states with least-stable site  $u = 2$ . All stable states must satisfy the inequality (B1), and in particular the right-hand side of it must be equal to  $x_2$ . This can only be the case if  $\sigma_2 = 0$  and  $\sigma_1 = 1$ ; i.e., the site 1 must belong to  $I^+[\sigma]$ . In terms of the order sequence  $p$ , this condition is equivalent to requiring that any element  $i$  without an overbar which is located to the left of element  $u$  must be assigned as  $\sigma_i = 1$ .

Likewise, in order to ensure that the left-hand side of the inequality (B1) is strictly less than its right-hand side, we require that any site  $j$  with an overbar to the right of element  $u$  must have  $\sigma_j = 0$ . In our example this requires that  $\sigma_4 = 0$ . Any site  $k$  left undetermined by these two conditions can be assigned as  $\sigma_k = 0$  or 1. In the above example these conditions leave the sites  $k = 3$  and 5 undetermined so that  $\mathcal{S}_{p,2}$  has four elements given by  $\mathcal{S}_{p,2} = \{(10000), (10100), (10001), (10101)\}$ . Repeating the construction for all values of  $u$ , the reader may verify that  $\mathcal{S}_p$  has 14 states in total. These are the states shown in Fig. 3.

In the following we will make repeated use of two results whose validity is a direct consequence of the construction of stable states given above. (i) Given a symbolic ordering sequence  $p$  and using Eq. (B1), the set of all stable genotypes  $\sigma$  can be inferred from it, and hence the possible pairs of least-stable sites  $(\ell, u)$  associated with these. (ii) Given any pair of sites  $\ell$  and  $u$  such that  $\bar{x}_\ell < x_u$ , there exists a symbolic ordering sequence  $p$  such that Eq. (B2) holds and thus  $\ell$  and  $u$  are the least-stable sites for some stable state  $\sigma$ . Whenever we assume that Eq. (B2) holds, this will imply that either we are given a specific order sequence  $p$  and that with respect to  $p$  the state  $\sigma$  is stable with  $(\ell, u)$  being the pair of least-stable sites, or alternatively, we are given  $(\ell, u)$  and consider the set of order sequences  $p$  and stable states  $\sigma$  compatible with this choice of least-stable sites. The particular point of view will be clear from the context.

### 3. Properties of secondary mutations

#### a. Secondary mutation must be complementary

We first derive some simple inequalities for the TIL model. The two properties given below follow immediately from assumptions (W1) and (W2) made above for  $w(x)$ :

$$x < x_i \Leftrightarrow w(x) > r_i w\left(\frac{x}{m_i}\right), \quad (\text{B8})$$

$$x > x_i \Leftrightarrow w(x) < r_i w\left(\frac{x}{m_i}\right). \quad (\text{B9})$$

Now, let  $\sigma$  be a stable state, such that Eq. (B2) holds. Then, we can show from the previous results that for all  $i \in I^-[\sigma] \setminus \{u\}$ ,

$$\frac{f_{\sigma^{+u,i}}(x^+[\sigma])}{f_{\sigma^{+u}}(x^+[\sigma])} < 1, \quad (\text{B10})$$

and for all  $j \in I^+[\sigma] \setminus \{\ell\}$ ,

$$\frac{f_{\sigma^{-\ell,j}}(x^-[\sigma])}{f_{\sigma^{-\ell}}(x^-[\sigma])} < 1. \quad (\text{B11})$$

The last two inequalities together assert that first secondary mutations which are in the same direction as the primary mutation are fitness decreasing. Thus, either the first mutation leads to a LFM, and hence there will be no further mutations, or the first secondary mutation must be complementary to the original mutation.

#### b. Locations of complementary secondary mutations

Let  $\sigma$  be a stable state such that Eq. (B2) holds. Then for  $i \in I^+[\sigma]$ ,

$$\bar{x}_i > \bar{x}_u \Leftrightarrow \frac{f_{\sigma^{+u,i}}(x^+[\sigma])}{f_{\sigma^{+u}}(x^+[\sigma])} > 1. \quad (\text{B12})$$

Therefore, subsequent to an initial mutation under concentration increase at site  $u$ , fitness-increasing complementary mutation sites are those sites  $i \in I^+[\sigma]$  for which the symbol  $\bar{i}$  is located to the right of  $\bar{u}$  in the order sequence  $p$ . Note, in particular, that the initial mutation site  $u$  itself cannot also be the site for a subsequent secondary mutation, as this would have implied that  $\sigma$  has a higher fitness than  $\sigma^{+u}$  at the triggering concentration.

Likewise, for  $j \in I^-[\sigma]$ ,

$$x_j < x_\ell \Leftrightarrow \frac{f_{\sigma^{-\ell,j}}(x^-[\sigma])}{f_{\sigma^{-\ell}}(x^-[\sigma])} > 1. \quad (\text{B13})$$

Any secondary mutation following an initial mutation under concentration decrease at site  $\ell$  must be a site  $j \in I^-[\sigma]$  located to the left of  $\ell$  in the symbolic order sequence  $p$ . The statements Eqs. (B12) and (B13) are proven by repeated application of Eqs. (B8) and (B9) and the properties of ordering sequences  $p$  that are compatible with the assumption Eq. (B2).

### c. Secondary mutations cannot cause transitions to a subset or superset

Assume the contrary. Then, according to the property of directed path accessibility, a path must exist where the first secondary mutation is in the same direction as the original mutation. But this is not possible according to the previous result.

### d. Conditions for the absence of secondary mutations

Consider a realization of the TIL model with  $L$  sites and let  $\sigma$  be a stable state satisfying Eq. (B2). Assume that we are given a symbolic ordering sequence  $p$  compatible with Eq. (B2). For any site  $u = 1, 2, \dots, L$ , we will be interested in the interval of elements of  $p$  that is bounded to the left by  $\bar{u}$  and to the right by  $u$ . Denote by  $\mathcal{I}_u$  the set of sites  $j$  that appear in this interval without overbars. Likewise, let  $\bar{\mathcal{I}}_u$  be the set of sites that appear in this interval with overbars. Our definition is such that neither of the two sets of sites  $\mathcal{I}_u$  and  $\bar{\mathcal{I}}_u$  contain  $u$ .

Consider now transitions out of  $\sigma$  under concentration increases. By assumption, under a concentration increase to (a value slightly above)  $x^+[\sigma]$ , the site  $u$  will mutate first,  $\sigma_u = 0 \rightarrow 1$ , leading to  $\sigma^{+u}$ , and as a result, the upper limit of the stability range of  $\sigma^{+u}$  increases to  $x^+[\sigma^{+u}] > x^+[\sigma]$ . In order to assert the stability of  $\sigma^{+u}$  at the concentration  $x^+[\sigma]$  which triggered the mutation at  $u$ , we must require that

$$x^-[\sigma^{+u}] \leq x^+[\sigma]. \quad (\text{B14})$$

If this condition is not satisfied, then  $x^\pm[\sigma^{+u}] > x^+[\sigma]$ , and at least one secondary mutation occurs. We thus need to find conditions under which Eq. (B14) holds.

Now in terms of the ordering sequence  $p$ , the site  $\bar{\ell}$  must be located to the left of  $u$ , as must be the site  $\bar{u}$ . Moreover, since  $\ell$  and  $u$  have to be distinct,  $\bar{\ell}$  is either to the left or right of  $\bar{u}$ . In the former case we have  $\bar{x}_\ell < \bar{x}_u$ , and hence,

$$x^-[\sigma^{+u}] = m_{\sigma^{+u}} \bar{x}_u = m_\sigma x_u = x^+[\sigma]. \quad (\text{B15})$$

Since Eq. (B14) is satisfied, genotype  $\sigma^{+u}$  is a local fitness maximum at this concentration and there will therefore be no secondary mutations. Suppose next that  $\bar{x}_\ell > \bar{x}_u$ . In this case,

$$x^-[\sigma^{+u}] = m_{\sigma^{+u}} \bar{x}_\ell = m_\sigma \frac{\bar{x}_\ell}{\bar{x}_u} x_u > x^+[\sigma]. \quad (\text{B16})$$

Therefore there will be at least one complementary secondary mutation at some site  $i \in I^+[\sigma]$ . Condition Eq. (B12) asserts that in order for such a mutation to be fitness increasing,  $i$  must be such that  $\bar{x}_i > \bar{x}_u$ . Using Eq. (B1), it follows that the stability condition of  $\sigma$ , as given by Eq. (B2), implies that  $\bar{x}_i < x_u$ , so that the secondary

mutation site must be contained in the set  $\bar{\mathcal{I}}_u$ . Note in particular that the site  $\ell$  itself satisfies these conditions and hence is a possible candidate for the first secondary mutation.

Combining all of the above results, under increasing concentration, a secondary mutation will occur, if and only if the set  $\bar{\mathcal{I}}_u$  is nonempty, and the state  $\sigma$  is such that for some  $j \in \bar{\mathcal{I}}_u$  we have  $\sigma_j = 1$ . Conversely, a secondary mutation will *not* occur if and only if one of the following two conditions holds.

- (U1) The set  $\bar{\mathcal{I}}_u$  is empty.
- (U2) The set  $\bar{\mathcal{I}}_u$  is nonempty, and the state  $\sigma$  is such that for each  $j \in \bar{\mathcal{I}}_k$  we have  $\sigma_j = 0$ .

In a similar manner, one can show that under decreasing concentration a secondary mutation will not occur, if and only if one of the following two conditions holds.

- (D1) The set  $\mathcal{I}_\ell$  is empty.
- (D2) The set  $\mathcal{I}_\ell$  is nonempty, and the state  $\sigma$  is such that for each  $j \in \mathcal{I}_\ell$  we have  $\sigma_j = 1$ .

Observe now that in order for secondary mutations to be absent from all transitions in a TIL model, the sets  $\mathcal{I}_k$  and  $\bar{\mathcal{I}}_k$  have to be empty for each  $k = 1, 2, \dots, L$ , since otherwise there will exist stable states for which conditions (U2) or (D2) can be made not to hold. The only ordering sequence for which both of these sets are empty for each  $k$  is the sequence

$$p = \bar{1} \ 1 \ \bar{2} \ 2 \ \dots \ \bar{L} \ L.$$

## APPENDIX C: STATISTICAL RESULTS

Herein, we derive the statistical results discussed in the main body of the paper.

### 1. Probability density function used in the numerics

We assume that the dose-response curve is of Hill type with  $n = 2$ . In order to satisfy the requirement (W2) for the dose-response function, the parameters  $(r_j, m_j)$  must be chosen such that  $m_j^2 r_j > 1$  for each  $j = 1, 2, \dots, L$ . We further assume that the pairs  $(r_j, m_j)$  are independently and identically distributed, so that their joint density is given by  $Q(\{r_i, m_i\}) = \prod_{j=1}^L P(r_j, m_j)$ . We write  $P(r_j, m_j) = P_1(r_j)P_2(m_j|r_j)$ . We chose

$$P_1(r) = \sqrt{\frac{2}{\pi}} \frac{e^{-(\ln r)^2/2}}{r} \quad (\text{C1})$$

$$P_2(m|r) = \mathcal{N} \left( \frac{e^{-(\ln m)^2/2}}{m} \Theta \left( m - \frac{1}{\sqrt{r}} \right) \right), \quad (\text{C2})$$

where  $\Theta(\cdot)$  is the Heaviside step function and  $\mathcal{N}$  is the appropriate normalization constant. This choice is for ease of implementation. A similar model was used in Ref. [23].

## 2. Asymptotic number of stable states

Consider a genotype  $\sigma$  with  $n$  mutations; i.e.,  $\sum_i \sigma_i = n$ . The number of such genotypes is  $\binom{L}{n}$  and such a  $\sigma$  is a stable state if Eq. (B1) holds. Since  $x_i$  and  $\bar{x}_i$  are independent for distinct sites, the probability density that the left-hand side of Eq. (B1) is less than  $z$  and the right-hand side is greater than  $z$  is  $(d/dz)F_{\bar{x}}^{L-n}(z)[1 - F_x(z)]^n$ . Then the mean number of stable states is

$$\begin{aligned} \langle N_{ss} \rangle &= \sum_{n=0}^L \binom{L}{n} \int dz \left[ \frac{d}{dz} F_{\bar{x}}^{L-n}(z) \right] [1 - F_x(z)]^n \\ &= L \int dz [1 - F_x(z) + F_{\bar{x}}(z)]^{L-1} F'_{\bar{x}}(z), \end{aligned} \quad (\text{C3})$$

from which the result in the main text follows using a saddle point approximation for  $L$  large.

## 3. Asymptotic approximation for number of mutations

The fitness  $f$  of a genotype  $\sigma$  can be expressed as

$$\ln f = \sum_i \sigma_i \ln r_i - \ln(1 + x^2 e^{-2 \sum_i \sigma_i \ln m_i}). \quad (\text{C4})$$

The number of mutations in the genotype is  $n = \sum_i \sigma_i$ . A simple heuristic that produces good approximations for the mean of various quantities at large  $L$  is as follows: we consider the fitness of a genotype to be a function of  $x$  and  $n$  only, and replace the parameters associated with the mutations by suitable averages. Thus, we write Eq. (C4) as

$$\ln f(n) \simeq -na - \ln(1 + x^2 e^{-2nb}), \quad (\text{C5})$$

where  $a = -\langle \ln r \rangle$  and  $b = \langle \ln m \rangle$ . For any given  $x$ , one can now maximize Eq. (C5) with respect to  $n$ , yielding an approximation to the mean mutation number at  $x$  for stable maxima. Taking the derivative of the above with respect to  $n$  and setting it to zero produces the equation:

$$\frac{2bx^2 e^{-2nb}}{1 + x^2 e^{-2nb}} = a.$$

The solution to this is

$$n = \frac{\ln x}{b} + \frac{1}{2b} \ln \left( \frac{2b}{a} - 1 \right). \quad (\text{C6})$$

For large  $x$  and therefore large  $n$ , the leading order is

$$n \simeq \frac{\ln x}{b}. \quad (\text{C7})$$

This estimate works well when  $L$  is large and  $1 \ll [\ln(x)/\langle \ln m \rangle] \ll L$ .

- [1] S. Wright, *The Roles of Mutation, Inbreeding, Crossbreeding, and Selection in Evolution*, in *Proceedings of the Sixth International Congress on Genetics, 1932* (Brooklyn Botanic Garden, Brooklyn, NY, 1932), Vol. 1, pp. 356–366.
- [2] D. M. Weinreich, N. F. Delaney, M. A. DePristo, and D. L. Hartl, *Darwinian Evolution Can Follow Only Very Few Mutational Paths to Fitter Proteins*, *Science* **312**, 111 (2006).
- [3] E. R. Lozovsky, T. Chookajorn, K. M. Brown, M. Imwong, P. J. Shaw, S. Kamchonwongpaisan, D. E. Neafsey, D. M. Weinreich, and D. L. Hartl, *Stepwise Acquisition of Pyrimethamine Resistance in the Malaria Parasite*, *Proc. Natl. Acad. Sci. U.S.A.* **106**, 12025 (2009).
- [4] M. F. Schenk, I. G. Szendro, M. L. M. Salverda, J. Krug, and J. A. G. M. de Visser, *Patterns of Epistasis between Beneficial Mutations in an Antibiotic Resistance Gene*, *Mol. Biol. Evol.* **30**, 1779 (2013).
- [5] J. A. G. M. de Visser and J. Krug, *Empirical Fitness Landscapes and the Predictability of Evolution*, *Nat. Rev. Genet.* **15**, 480 (2014).
- [6] A. C. Palmer, E. Toprak, M. Baym, S. Kim, A. Veres, S. Bershtein, and R. Kishony, *Delayed Commitment to Evolutionary Fate in Antibiotic Resistance Fitness Landscapes*, *Nat. Commun.* **6**, 1 (2015).
- [7] C. Bank, S. Matuszewski, R. T. Hietpas, and J. D. Jensen, *On the (Un)predictability of a Large Intragenic Fitness Landscape*, *Proc. Natl. Acad. Sci. U.S.A.* **113**, 14085 (2016).
- [8] J. Domingo, G. Diss, and B. Lehner, *Pairwise and Higher-Order Genetic Interactions during the Evolution of a tRNA*, *Nature (London)* **558**, 117 (2018).
- [9] I. Fragata, A. Blanckaert, M. A. D. Louro, D. A. Liberles, and C. Bank, *Evolution in the Light of Fitness Landscape Theory*, *Trends Ecol. Evol.* **34**, 69 (2019).
- [10] V. O. Pokusaeva, D. R. Usmanova, E. V. Putintseva, L. Espinar, K. S. Sarkisyan, A. S. Mishin, N. S. Bogatyreva, D. N. Ivankov, A. V. Akopyan, S. Y. Avvakumov, I. S. Povolotskaya, G. J. Filion, L. B. Carey, and F. A. Kondrashov, *An Experimental Assay of the Interactions of Amino Acids from Orthologous Sequences Shaping a Complex Fitness Landscape*, *PLoS Genet.* **15**, e1008079 (2019).
- [11] J. Franke, A. Klözer, J. A. G. M. de Visser, and J. Krug, *Evolutionary Accessibility of Mutational Pathways*, *PLoS Comput. Biol.* **7**, e1002134 (2011).
- [12] I. G. Szendro, M. F. Schenk, J. Franke, J. Krug, and J. A. G. M. de Visser, *Quantitative Analyses of Empirical Fitness Landscapes*, *J. Stat. Mech.* (2013) P01005.
- [13] J. Neidhart, I. G. Szendro, and J. Krug, *Adaptation in Tunably Rugged Fitness Landscapes: The Rough Mount Fuji Model*, *Genetics* **198**, 699 (2014).
- [14] L. Ferretti, B. Schmiegel, D. Weinreich, A. Yamauchi, Y. Kobayashi, F. Tajima, and G. Achaz, *Measuring Epistasis in Fitness Landscapes: The Correlation of Fitness Effects of Mutations*, *J. Theor. Biol.* **396**, 132 (2016).
- [15] F. Blanquart and T. Bataillon, *Epistasis and the Structure of Fitness Landscapes: Are Experimental Fitness Landscapes Compatible with Fisher's Geometric Model?*, *Genetics* **203**, 847 (2016).



- [16] K. Crona, A. Gavryushkin, D. Greene, and N. Beerenwinkel, *Inferring Genetic Interactions from Comparative Fitness Data*, *eLife* **6**, e28629 (2017).
- [17] A. Murugan, K. Husain, M. J. Rust, C. Hepler, J. Bass, J. M. Pietsch, P. S. Swain, S. G. Jena, J. E. Toettcher, A. K. Chakraborty *et al.*, *Roadmap on Biology in Time Varying Environments*, *Phys. Biol.* **18**, 041502 (2021).
- [18] M. G. J. de Vos, S. E. Schoustra, and J. A. G. M. de Visser, *Ecology Dictates Evolution? About the Importance of Genetic and Ecological Constraints in Adaptation*, *Europhys. Lett.* **122**, 58002 (2018).
- [19] F. A. Gorter, M. G. M. Aarts, B. J. Zwaan, and J. A. G. M. de Visser, *Local Fitness Landscapes Predict Yeast Evolutionary Dynamics in Directionally Changing Environments*, *Genetics* **208**, 307 (2018).
- [20] D. W. Anderson, F. Baier, G. Yang, and N. Tokuriki, *The Adaptive Landscape of a Metallo-Enzyme Is Shaped by Environment-Dependent Epistasis*, *Nat. Commun.* **12**, 3867 (2021).
- [21] P. M. Mira, J. C. Meza, A. Nandipati, and M. Barlow, *Adaptive Landscapes of Resistance Genes Change as Antibiotic Concentrations Change*, *Mol. Biol. Evol.* **32**, 2707 (2015).
- [22] C. B. Ogbunugafor, C. S. Wylie, I. Diakite, D. M. Weinreich, and D. L. Hartl, *Adaptive Landscape by Environmental Interactions Dictate Evolutionary Dynamics in Models of Drug Resistance*, *PLoS Comput. Biol.* **12**, e1004710 (2016).
- [23] S. G. Das, S. O. Direito, B. Waclaw, R. J. Allen, and J. Krug, *Predictable Properties of Fitness Landscapes Induced by Adaptational Tradeoffs*, *eLife* **9**, e55155 (2020).
- [24] D. W. Kolpin, M. Skopec, M. T. Meyer, E. T. Furlong, and S. D. Zaugg, *Urban Contribution of Pharmaceuticals and Other Organic Wastewater Contaminants to Streams during Differing Flow Conditions*, *Sci. Total Environ.* **328**, 119 (2004).
- [25] D. I. Andersson and D. Hughes, *Microbiological Effects of Sublethal Levels of Antibiotics*, *Nat. Rev. Microbiol.* **12**, 465 (2014).
- [26] R. A. Fisher, *The Genetical Theory of Natural Selection* (Dover, New York, 1958).
- [27] E. V. Koonin, *The Logic of Chance: The Nature and Origin of Biological Evolution* (FT Press Science, Upper Saddle River, NJ, 2011).
- [28] G. Sella and A. E. Hirsh, *The Application of Statistical Physics to Evolutionary Biology*, *Proc. Natl. Acad. Sci. U.S.A.* **102**, 9541 (2005).
- [29] M. Manhart and A. V. Morozov, *Statistical Physics of Evolutionary Trajectories on Fitness Landscapes, First-Passage Phenomena and Their Applications* (World Scientific, Singapore, 2014), pp. 416–446.
- [30] S. Hwang, B. Schmiegel, L. Ferretti, and J. Krug, *Universality Classes of Interaction Structures for NK Fitness Landscapes*, *J. Stat. Phys.* **172**, 226 (2018).
- [31] D. L. Stein, *Spin Glasses and Biology* (World Scientific, Singapore, 1992).
- [32] S. Franz, L. Peliti, and M. Sellitto, *An Evolutionary Version of the Random Energy Model*, *J. Phys. A* **26**, L1195 (1993).
- [33] C. E. Maloney and A. Lemaître, *Amorphous Systems in Athermal, Quasistatic Shear*, *Phys. Rev. E* **74**, 016118 (2006).
- [34] N. C. Keim, J. D. Paulsen, Z. Zeravcic, S. Sastry, and S. R. Nagel, *Memory Formation in Matter*, *Rev. Mod. Phys.* **91**, 035002 (2019).
- [35] M. Mungan, S. Sastry, K. Dahmen, and I. Regev, *Networks and Hierarchies: How Amorphous Materials Learn to Remember*, *Phys. Rev. Lett.* **123**, 178002 (2019).
- [36] R. P. Behringer and B. Chakraborty, *The Physics of Jamming for Granular Materials: A Review*, *Rep. Prog. Phys.* **82**, 012601 (2019).
- [37] D. Bonn, M. M. Denn, L. Berthier, T. Divoux, and S. Manneville, *Yield Stress Materials in Soft Condensed Matter*, *Rev. Mod. Phys.* **89**, 035005 (2017).
- [38] I. Regev, T. Lookman, and C. Reichhardt, *Onset of Irreversibility and Chaos in Amorphous Solids under Periodic Shear*, *Phys. Rev. E* **88**, 062401 (2013).
- [39] D. Fiocco, G. Foffi, and S. Sastry, *Oscillatory Athermal Quasistatic Deformation of a Model Glass*, *Phys. Rev. E* **88**, 020301(R) (2013).
- [40] M. Mungan and M. M. Terzi, *The Structure of State Transition Graphs in Hysteresis Models with Return Point Memory: I. General Theory*, *Ann. Inst. Henri Poincaré* **20**, 2819 (2019).
- [41] M. Mungan and T. A. Witten, *Cyclic Annealing as an Iterated Random Map*, *Phys. Rev. E* **99**, 052132 (2019).
- [42] I. Regev, I. Attia, K. Dahmen, S. Sastry, and M. Mungan, *Topology of the Energy Landscape of Sheared Amorphous Solids and the Irreversibility Transition*, *Phys. Rev. E* **103**, 062614 (2021).
- [43] N. C. Keim and J. D. Paulsen, *Multiperiodic Orbits from Interacting Soft Spots in Cyclically Sheared Amorphous Solids*, *Sci. Adv.* **7**, eabg7685 (2021).
- [44] F. Preisach, *Über die Magnetische Nachwirkung*, *Z. Phys.* **94**, 277 (1935).
- [45] O. Hovorka and G. Friedman, *Onset of Reptations and Critical Hysteretic Behavior in Disordered Systems*, *J. Magn. Magn. Mater.* **290**, 449 (2005).
- [46] C. W. Lindeman and S. R. Nagel, *Multiple Memory Formation in Glassy Landscapes*, *Sci. Adv.* **7**, eabg7133 (2021).
- [47] M. van Hecke, *Profusion of Transition Pathways for Interacting Hysterons*, *Phys. Rev. E* **104**, 054608 (2021).
- [48] H. Bense and M. van Hecke, *Complex Pathways and Memory in Compressed Corrugated Sheets*, *Proc. Natl. Acad. Sci. U.S.A.* **118**, e2111436118 (2021).
- [49] G. Chevereau, M. Dravecká, T. Batur, A. Guvenek, D. H. Ayhan, E. Toprak, and T. Bollenbach, *Quantifying the Determinants of Evolutionary Dynamics Leading to Drug Resistance*, *PLOS Biol.* **13**, e1002299 (2015).
- [50] M. Lukačičinová, B. Fernando, and T. Bollenbach, *Highly Parallel Lab Evolution Reveals that Epistasis Can Curb the Evolution of Antibiotic Resistance*, *Nat. Commun.* **11**, 3105 (2020).
- [51] R. R. Regoes, C. Wiuff, R. M. Zappala, K. N. Garner, F. Baquero, and B. R. Levin, *Pharmacodynamic Functions: A Multiparameter Approach to the Design of Antibiotic Treatment Regimens*, *Antimicrob. Agents Chemother.* **48**, 3670 (2004).
- [52] L. L. Marcusson, N. Frimodt-Møller, and D. Hughes, *Interplay in the Selection of Fluoroquinolone Resistance and Bacterial Fitness*, *PLoS Pathogens* **5**, e1000541 (2009).

- [53] M. Knopp and D. I. Andersson, *Predictable Phenotypes of Antibiotic Resistance Mutations*, *mBio* **9**, e00770 (2018).
- [54] A. H. Melnyk, A. Wong, and R. Kassen, *The Fitness Costs of Antibiotic Resistance Mutations*, *Evolut. Appl.* **8**, 273 (2015).
- [55] K. Crona, D. Greene, and M. Barlow, *The Peaks and Geometry of Fitness Landscapes*, *J. Theor. Biol.* **317**, 1 (2013).
- [56] S. Kauffman and S. Levin, *Towards a General Theory of Adaptive Walks on Rugged Landscapes*, *J. Theor. Biol.* **128**, 11 (1987).
- [57] H. A. Orr, *The Population Genetics of Adaptation: The Adaptation of DNA Sequences*, *Evolution* **56**, 1317 (2002).
- [58] S. Seetharaman and K. Jain, *Adaptive Walks and Distribution of Beneficial Fitness Effects*, *Evolution* **68**, 965 (2014).
- [59] A. Agarwala and D. S. Fisher, *Adaptive Walks on High-Dimensional Fitness Landscapes and Seascapes with Distance-Dependent Statistics*, *Theor. Popul. Biol.* **130**, 13 (2019).
- [60] D. R. Rokyta, P. Joyce, S. B. Caudle, and H. A. Wichman, *An Empirical Test of the Mutational Landscape Model of Adaptation Using a Single-Stranded DNA Virus*, *Nat. Genet.* **37**, 441 (2005).
- [61] D. R. Rokyta, Z. Abdo, and H. A. Wichman, *The Genetics of Adaptation for Eight Microvirid Bacteriophages*, *J. Mol. Evol.* **69**, 229 (2009).
- [62] S. E. Schoustra, T. Bataillon, D. R. Gifford, and R. Kassen, *The Properties of Adaptive Walks in Evolving Populations of Fungus*, *PLOS Biol.* **7**, e1000250 (2009).
- [63] D. M. Weinreich, R. A. Watson, and L. Chao, *Perspective: Sign Epistasis and Genetic Constraint on Evolutionary Trajectories*, *Evolution* **59**, 1165 (2005).
- [64] M. M. Terzi and M. Mungan, *State Transition Graph of the Preisach Model and the Role of Return-Point Memory*, *Phys. Rev. E* **102**, 012122 (2020).
- [65] H. Teotónio and M. R. Rose, *Perspective: Reverse Evolution*, *Evolution* **55**, 653 (2001).
- [66] J. T. Bridgham, E. A. Ortlund, and J. W. Thornton, *An Epistatic Ratchet Constrains the Direction of Glucocorticoid Receptor Evolution*, *Nature (London)* **461**, 515 (2009).
- [67] M. Kaltenbach, C. J. Jackson, E. C. Campbell, F. Hollfelder, and N. Tokuriki, *Reverse Evolution Leads to Genotypic Incompatibility Despite Functional and Active Site Convergence*, *eLife* **4**, e06492 (2015).
- [68] D. I. Andersson and D. Hughes, *Antibiotic Resistance and Its Cost: Is It Possible to Reverse Resistance?*, *Nat. Rev. Microbiol.* **8**, 260 (2010).
- [69] R. C. Allen, J. Engelstädter, S. Bonhoeffer, B. A. McDonald, and A. R. Hall, *Reversing Resistance: Different Routes and Common Themes across Pathogens*, *Proc. R. Soc. B* **284**, 20171619 (2017).
- [70] P. Durão, R. Balbontín, and I. Gordo, *Evolutionary Mechanisms Shaping the Maintenance of Antibiotic Resistance*, *Trends Microbiol.* **26**, 677 (2018).
- [71] A. Dunai, R. Spohn, Z. Farkas, V. Lázár, Á. Györkei, G. Apjok, G. Boross, B. Szappanos, G. Grézal, A. Faragó *et al.*, *Rapid Decline of Bacterial Drug-Resistance in an Antibiotic-Free Environment through Phenotypic Reversion*, *eLife* **8**, e47088 (2019).
- [72] P. S. Zur Wiesch, J. Engelstädter, and S. Bonhoeffer, *Compensation of Fitness Costs and Reversibility of Antibiotic Resistance Mutations*, *Antimicrob. Agents Chemother.* **54**, 2085 (2010).
- [73] J. P. Sethna, K. Dahmen, S. Kartha, J. A. Krumhansl, B. W. Roberts, and J. D. Shore, *Hysteresis and Hierarchies: Dynamics of Disorder-Driven First-Order Phase Transformations*, *Phys. Rev. Lett.* **70**, 3347 (1993).
- [74] M. Baym, T. D. Lieberman, E. D. Kelsic, R. Chait, R. Gross, I. Yelin, and R. Kishony, *Spatiotemporal Microbial Evolution on Antibiotic Landscapes*, *Science* **353**, 1147 (2016).
- [75] M. F. Schenk, M. P. Zwart, S. Hwang, P. Ruelens, E. Severing, J. Krug, and J. De Visser, *Population Size Mediates the Contribution of High-Rate and Large-Benefit Mutations to Parallel Evolution*, *Nat. Ecol. Evol.* **6**, 439 (2022).
- [76] A. E. Lobkovsky and E. V. Koonin, *Replaying the Tape of Life: Quantification of the Predictability of Evolution*, *Front. Genet.* **3**, 246 (2012).
- [77] P. M. Mira, K. Crona, D. Greene, J. C. Meza, B. Sturmfels, and M. Barlow, *Rational Design of Antibiotic Treatment Plans: A Treatment Strategy for Managing Evolution and Reversing Resistance*, *PLoS One* **10**, e0122283 (2015).
- [78] D. Nichol, P. Jeavons, A. G. Fletcher, R. A. Bonomo, P. K. Maini, J. L. Paul, R. A. Gatenby, A. R. Anderson, and J. G. Scott, *Steering Evolution with Sequential Therapy to Prevent the Emergence of Bacterial Antibiotic Resistance*, *PLoS Comput. Biol.* **11**, e1004493 (2015).
- [79] J. H. Gillespie, *Molecular Evolution Over the Mutational Landscape*, *Evolution* **38**, 1116 (1984).
- [80] P. J. Gerrish and R. E. Lenski, *The Fate of Competing Beneficial Mutations in an Asexual Population*, *Genetica* **102**, 127 (1998).
- [81] M. Kimura, *On the Probability of Fixation of Mutant Genes in a Population*, *Genetics* **47**, 713 (1962).